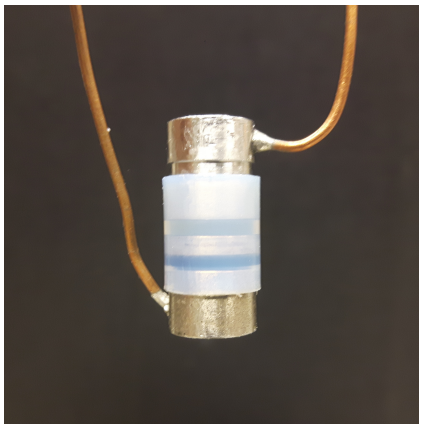
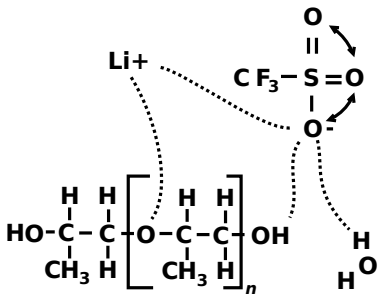
CHALMERS
UNIVERSITY OF TECHNOLOGY






# Influence of Water on Poly(propylene glycol)-Lithium Triflate Electrolytes, Studied by Impedance and Infrared Spectroscopy

Master thesis in Physics and Astronomy

Erik OLANDER

Department of Physics
Chalmers University of Technology
Gothenburg, Sweden 2019

Influence of Water on Poly(propylene glycol)-Lithium Triflate Electrolytes, Studied by Impedance and Infrared Spectroscopy
Master thesis in Physics and Astronomy
©Erik Olander 2019,
Pictures: ©Erik Olander 2019 CC BY-SA 4.0
Department of Physics
Chalmers University of Technology
Gothenburg, Sweden 2019

Front page pictures: impedance measuring electrode, diagram of important molecular interactions. ©Erik Olander 2019

A big thank you to everyone in the Electro-Physics group.

# 1 Abstract

In this thesis, Poly(propylene glycol)4000-$LiCF_3SO_3$-water electrolytes were studied with thermogravimetry, impedance and infrared spectroscopy. A method for drying the compounds and adding water was developed successfully. Among the samples without water, the medium concentration 0.63 mol/kg $LiCF_3SO_3$ (LiTf) had the highest conductivity of $2.9 \cdot 10^{-4}$ S/m. Water increased the conductivity for all samples. The conductivity increased the most for the high concentration 2.7 mol/kg LiTf sample, from $8.4 \cdot 10^{-6}$ S/m dry to $1.5 \cdot 10^{-2}$ S/m wet. Water in PPG4000 above saturation separates into a wet polymer phase and an aqueous phase, but LiTf enables more water to be mixed into the electrolyte without phase separation. The limited molecular interaction between PPG4000 chain and water explains the phase separation. The PPG4000 hydrophilic OH endgroups can explain the ability to form emulsion with water. The $SO_3$ 1041 $cm^{-1}$ and 1031 $cm^{-1}$ symmetric stretch IR bands show that OH and $Li^+$ compete in interacting with $SO_3$. The ion pair dissociation could explain part of the conductivity increase with added water.

Keywords: Polymer electrolytes, Impedance Spectroscopy, Conductivity, Permittivity, FTIR Infrared Spectroscopy, Lithium Triflate $LiCF_3SO_3$, Poly(propylene glycol) PPG PPG4000, Poly(propylene glycol)-Water Mixtures, Poly(propylene glycol)-Lithium Triflate electrolytes, Poly(propylene glycol)-Lithium Triflate-Water Mixtures, Macrophase and Microphase Separation, Phase Separation, Ion Pairs. Aqueous electrolytes.

# Contents


**1 Abstract** **1**

**2 Introduction** **4**

**3 Scope** **4**

**4 Background** **4**
4.1 Poly(propylene glycol) . . . . . 4
4.2 Lithium Triflate . . . . . 6
4.3 Water . . . . . 9
4.4 Ionic Solution theory . . . . . 9
4.5 Poly(propylene glycol) — Lithium Triflate Systems . . . . . 10
4.6 Electrolytes containing water . . . . . 11
4.7 Poly(propylene glycol) — Water systems . . . . . 11

**5 Method** **14**
5.1 Drying . . . . . 14
5.2 Sample Preparation . . . . . 15
5.3 Fourier Transform Infrared Spectroscopy . . . . . 17
5.4 Thermogravimetric analysis . . . . . 19
5.5 Impedance Spectroscopy . . . . . 19

**6 Experiment** **24**

**7 Results and Discussion** **25**
7.1 Thermogravimetric Measurements . . . . . 26
7.2 IR spectrum of PPG4000-Water . . . . . 29
7.3 IR spectrum of Lithium Triflate-Water . . . . . 30
7.4 PPG4000-LiTf-Water Equilibrium with Air . . . . . 32
7.5 Phase Separation of PPG4000-LiTf-Water . . . . . 33
7.6 IR spectrum of PPG4000-LiTf-Water . . . . . 37
7.7 Impedance Measurements . . . . . 42
7.8 Conductivity — Temperature Dependence . . . . . 44
7.8.1 Dry Samples . . . . . 44
7.8.2 Samples With Water . . . . . 44
7.9 Conductivity — LiTf Concentration dependence . . . . . 45
7.10 Conductivity — Water Content Dependence . . . . . 46
7.11 Complex Permittivity — Frequency Dependence . . . . . 48
7.12 Permittivity Value — LiTf and water concentration dependence 52

**8 Conclusion** **54**

**A Appendix** **56**
A.1 Method . . . . . 56
A.2 Code . . . . . 57

# 2 Introduction

Electrolytes have high ionic conductivity and negligible electronic conductivity. They are important for many electrochemical applications. A typical electrolyte is water with a salt dissolved in it. Water and other polar molecules are excellent solvents for salts. Polymer electrolytes have a further advantage that they can readily be made into a gel. Gels have an advantage compared to liquids in that they are more mechanically stable. Because water is contained in air it can contaminate electrolytes that are intended to be dry. It is therefore interesting to study how water containing electrolytes behave. Important properties that characterize an electrolyte are its conductivity and permittivity. The charge transport in an electrolyte comes from the mobility of the ion species, summed for all charge carriers. A prerequisite for this is that the ions are dissolved in the solvent. The solvent molecules shield the electrostatic field of the ions and thus lowers their chemical potential. An increase in number of dissolved ions will generally increase the ionic conductivity. Increased mobility such as from lowered viscosity will also increase the ionic conductivity. Polymer-salt-water electrolytes could have the benefit of combining the stability of gel polymer electrolytes and the high conductivity of aqueous electrolytes.

# 3 Scope

This project centers around the questions of

- How does water influence conductivity and permittivity of PPG-LiTf electrolytes.
- What does the conductivity, permittivity and IR spectrum say about PPG-LiTf-water systems?
- When and how does PPG-LiTf-water phase separate?
- How much does PPG-LiTf absorb or evaporate water?

# 4 Background

## 4.1 Poly(propylene glycol)

Poly(propylene glycol) or PPG is a colorless liquid polymer used in applications from industry to cosmetics. The polymer is made up of a polyether

Table 1: PPG4000 physical data [1].

| | |
|---|---|
| Viscosity (25 °C)(lit.) | 1.300 Pa·s |
| Density (25 °C) | 1.004 kg/l |

chain of $OCH(CH_3)CH_2$ repeating units, weighing 58.07 u. The PPG used in this project has OH endgroups. Figure 1 shows the chemical structure of PPG. The substance is liquid at room temperature despite its size. The weight average 4000 used in this study means that the polymers have an average of 69 repeating units. This also means that the ratio of OH end groups to the chain oxygen (the polyether oxygen) is 1:34. The OH end groups are more polar than the polyether chain, and will be more hydrophilic. The more polar ends will make the molecule a weak surfactant. The PPG4000 used in this study was chemical grade from Sigma Aldrich. The manufacturer measured the PPG4000 water content to <0.035% using the Karl Fisher method[1]. PPG4000 by its self is a poor electrical conductor. Table 1 shows data for PPG2000.

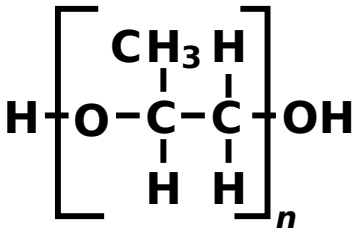



Figure 1: PPG chemical structure.

Table 2 shows literature values for the most prominent IR absorption bands of molecular groups also found in PPG4000. These wavenumbers are not specific to PPG4000 and thus approximate. Figure 2 shows the measured PPG4000 IR spectrum. PPG4000 $CH_3$ stretching bands are found between $2800\,\mathrm{cm}^{-1}$ and $3000\,\mathrm{cm}^{-1}$, the CO stretching and $CH_3$ bending bands are between $800\,\mathrm{cm}^{-1}$ and $1500\,\mathrm{cm}^{-1}$. The value $3471\,\mathrm{cm}^{-1}$ in Figure 2 for the OH band is very approximate.

Table 2: Literature values for IR bands of molecular groups also found in PPG4000.[2]

| Group | Wavenumber [$cm^{-1}$] |
|---|---|
| O-H Stretch | 3446 |
| Asymmetric $CH_3$ Stretch | 2970 |
| Symmetric $CH_3$ Stretch | 2890 |
| Asymmetric $CH_3$ Bending | 1450 |
| Symmetric $CH_3$ Bending | 1370 |
| Symmetric $CH_3$ Bending | 1350 |
| C-O Stretch | 1105 |

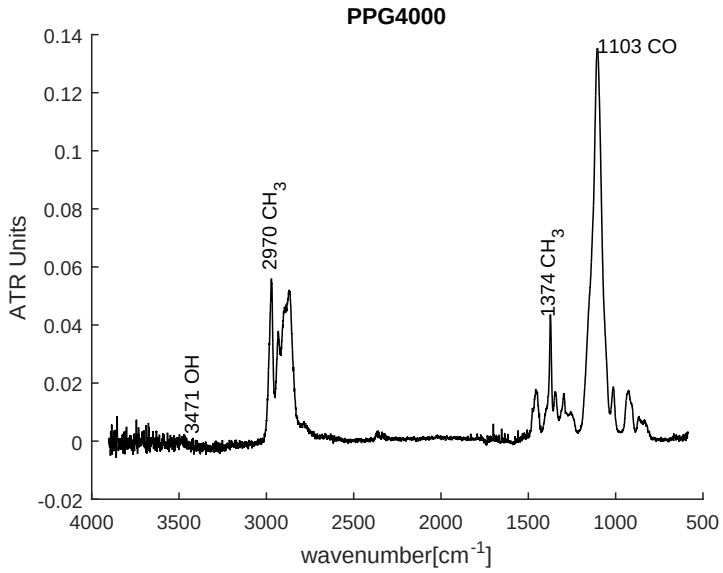



Figure 2: Measured IR spectrum of dry PPG4000 at room temperature. Only the strongest of the $CH_3$ bands is named in the figure due to their proximity.

.

## 4.2 Lithium Triflate

Litium triflouromethanesulfonate. $LiCF_3SO_3$ (LiTf) is a crystalline salt. Figure 3 shows its chemical structure. It is highly hygroscopic and will rapidly absorb water from the air, see Figure 4. When dissolved it has a cation $Li^+$ and an anion $CF_3SO_3^-$ ($Tf^-$). The molecular weight of LiTf is 156.01 u. This project used research grade LiTf from Sigma Aldrich[3]. Table 3 shows Tf-anion bands from literature. The measured IR spectrum is found in Figure 5. The 1222 $cm^{-1}$ and 1184 $cm^{-1}$ bands were not identified, but asymmetric $CF_3$ or $SO_3$ stretching are likely candidates.

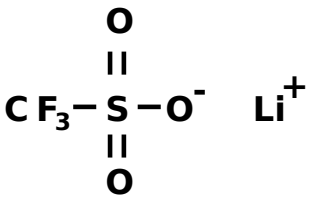


Figure 3: LiTf chemical structure.

Table 3: Approximate values of the LiTf IR bands according to literature[4][5].

| Group | Wavenumber [$cm^{-1}$] |
|---|---|
| Asymmetric $SO_3$ Stretch | 1300 |
| Asymmetric $CF_3$ Stretch | 1250 |
| Symmetric $SO_3$ Stretch | 1040 |
| Symmetric $CF_3$ Stretch | 760 |
| C-S Stretch | 640 |

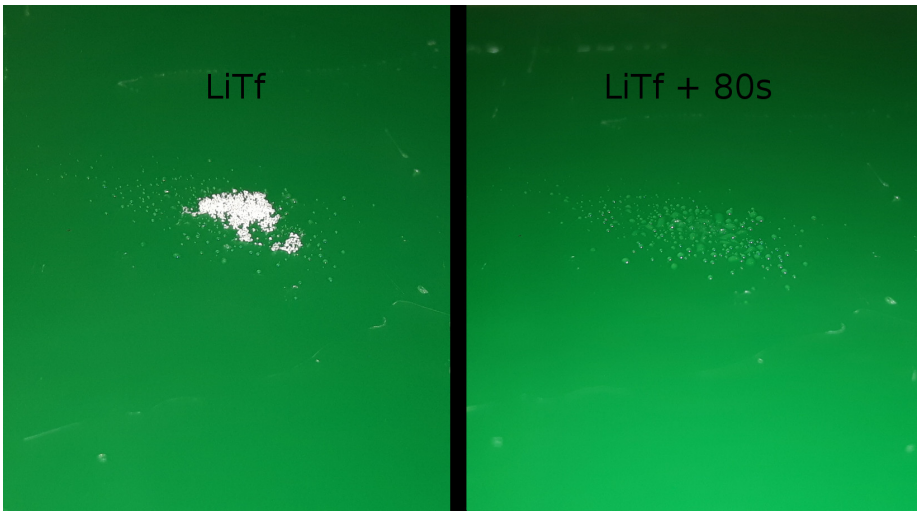



Figure 4: LiTf absorbs water from air humidity. In 80 s the LiTf has absorbed enough water to dissolve itself.

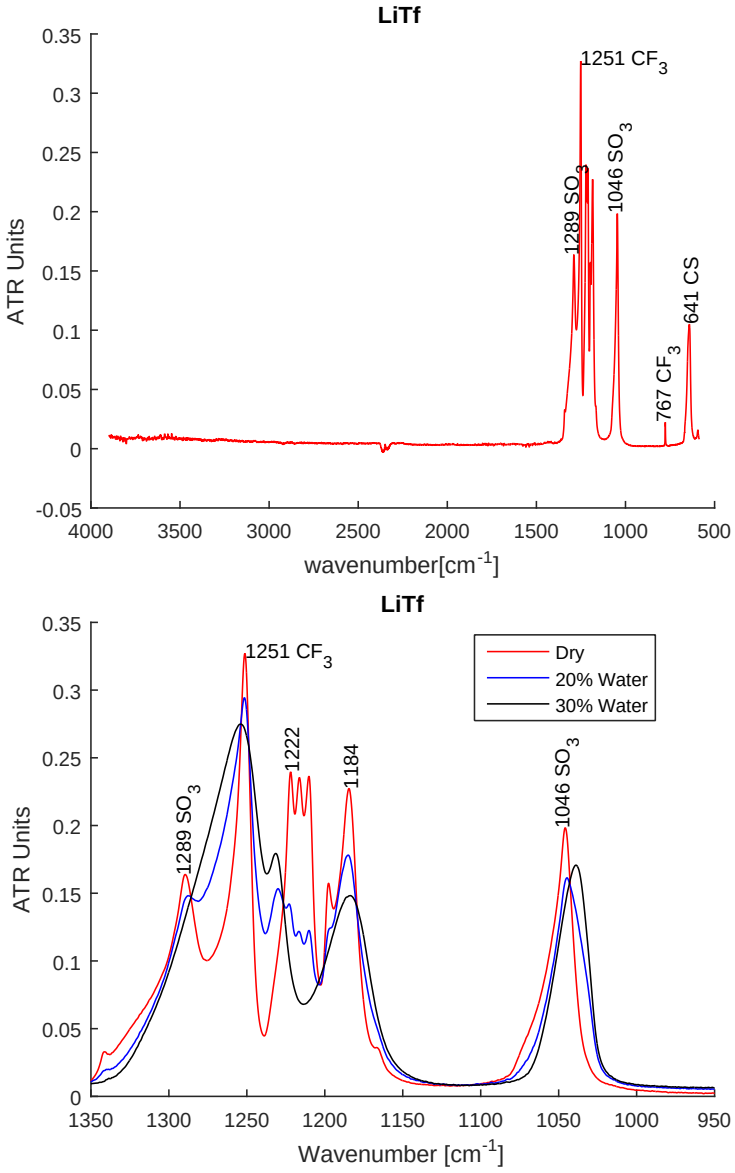



Figure 5: Measured IR spectrum of LiTf at room temperature. The lower graph is zoomed in and also shows the difference between wet and dry LiTf. The absorption bands are in the 600-1350 $\mathrm{cm}^{-1}$ range.

## 4.3 Water

Water will evaporate or condense depending of air humidity. A litre of air at 22 °C and 50 % humidity will hold 8 mg of vapor. Water has a high relative permittivity of 88 at room temperature[6]. Figure 6 shows the water IR spectrum, with the most prominent band at 3300 $\mathrm{cm}^{-1}$.

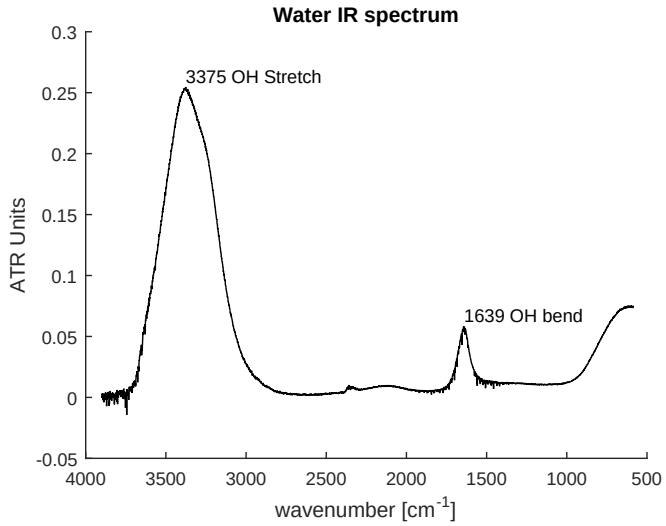



Figure 6: The IR spectrum of water at room temperature. In addition to the main absorption band between 3000 to 3800 $\mathrm{cm}^{-1}$, there are secondary bands at 1600 $\mathrm{cm}^{-1}$ and 500 $\mathrm{cm}^{-1}$.

## 4.4 Ionic Solution theory

An electrolyte is characterized by high ionic and negligible electron conductivity. It can be in liquid or solid state and a basic example is an ionic solution. An ionic solution can be described as ions surrounded by polarized molecules that lowers the ions electrical potential energy. Ions of opposite charge nearby an arbitrary central ion will make the overall charge of the ionic solution neutral. Relative movement of opposite ionic species will result in a current, with an associated conductivity. The molar conductivity $\Lambda$ is defined as the conductivity divided by the ion concentration, giving a measure of the effective activity of the ions. Experiments on diluted solutions give the semi-empirical relationship

$$\Lambda = \Lambda_0 - K\sqrt{c} \tag{1}$$

where $\Lambda$ is the molar conductivity, $c$ is the molality, $K$ is a constant, and $\Lambda_0$ is the molar conductivity at low concentrations[7].

Table 4: Table of ion complex properties for monovalent ions

| Ion Complex | Charge (±) | Dipole Moment |
|---|---|---|
| Free ion | 1 | very small |
| Ion pair | 0 | yes |
| Ion triplet | 1 | yes |
| n-ion complex | $<$ n | yes |

Two ions of opposite charge attract each other weakly despite being dissolved. If two ions form a weak bond they are said to form an ion pair. The formation of ion pairs will behave like an equilibrium reaction but have a lower energy than an ionic bond. Two ions will have two quantum mechanical states: one separated and one paired. The states will have different energies and a potential barrier between them. Ion pairs are charge neutral and the formation of ion pairs will lower the available charge carriers. This will lower the ionic conductivity. Ions can also form more complicated coordinations. Ion triplets will have two of one ion species and one ion of a opposite charge. All ion complexes with odd number of ions will have charge, as shown in Table 4.

To measure the conductivity with electrical equipment the electrolyte must be in contact with two electrical conductors, usually metallic. These electrical conductors are called an electrodes. The metal conductor will conduct electrons. If the electrodes are blocking and the potential moderate, the electrons will remain in the electrode. A build-up of electrons in the electrode and ions in the electrolyte will form a double layer. If the voltage is too high electrolysis reaction also occurs.

## 4.5 Poly(propylene glycol) — Lithium Triflate Systems

There are various ways to quantify the concentration of electrolytes. The most common ones are mass fraction, molar ratio, and molar mass concentration (molality). The mass fraction used the weight of water compared to the weight of the whole sample. The molecule weight $M$ relates mass fraction to molar ratio. $n$ is the amount of substance. The equality,

$$\frac{M_{PPG}}{M_{LiTf}}\frac{\varpi_{LiTf}}{1-\varpi_{LiTf}} = \frac{n_{LiTf}}{n_{PPG}}, \tag{2}$$

describes the relationship, where $\varpi$ is the weight fraction. From here it is straightforward to find the equation for the molality:

$$\frac{1}{M_{LiTf}}\frac{\varpi_{LiTf}}{1-\varpi_{LiTf}} = \frac{n_{LiTf}}{M_{PPG}n_{PPG}}. \tag{3}$$

Note that this equation gives molality in mol/g. Note that PPG is counted in repeating units.

## 4.6 Electrolytes containing water

For water-LiTf electrolytes to be used in batteries they have to be chemically stable. One aspect of this is the electrochemical stability window, the potential range where a molecule is neither oxidized nor reduced. A limit for using water in electrolytes is its low electrochemical stability window of 1.23 V. Lithium iron phosphate batteries for example have a nominal voltage of 3.2 V. This means that water is normally avoided in lithium ion batteries. Nevertheless water containing electrolytes are interesting from a research point of view. Recently Hamrin and Scott[8] showed that high concentrations of aqueous LiTf can reach an electrochemical stability window of 3.25 V.

## 4.7 Poly(propylene glycol) — Water systems

The solubility of PPG4000 in water is negligible <0.01%[1]. However PPG4000 dissolves approximately 4% water. Figure 7 shows the contrast to PPG400 which is water soluble[1]. For PPG4000, concentrations between 4% and 100% water will cause phase separation as shown in Figure 8. The wet PPG4000 appears as a milky emulsion. This state can be created by stirring, but appeared on its own in this case. An analysis of this phenomenon is beyond the scope of this thesis, but the surfactant property of PPG4000 could explain emulsion forming. Table 5 from literature[10] shows how the permittivity of PPG water mixtures increases with water content.

Table 5: Relative permittivity of PPG2000-Water.[10]

| | |
|---|---|
| PPG2000 | 5.6 |
| PPG2000, 25% water vol | 8.9 |
| PPG2000, 55% water vol | 34.1 |
| water | 82.3 |

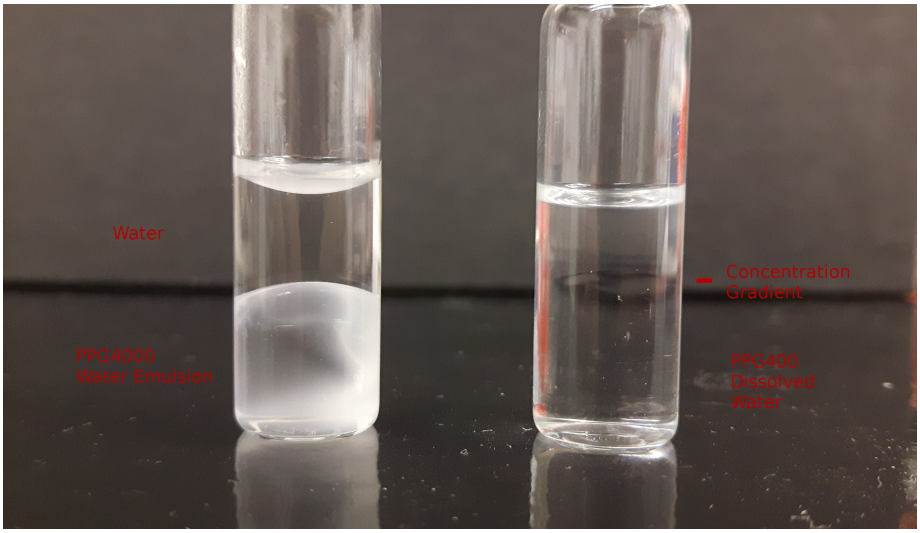



Figure 7: Water doesn't dissolve PPG4000, but PPG4000 forms an emulsion with water. PPG400 and water dissolve each other, but don't mix completely.




Figure 8: PPG4000 and water form macrophase and microphase separation. The water PPG4000 interface has a significant contact angle. The two liquids have very similar density. The PPG4000 next to the water will after time become milky.

# 5 Method

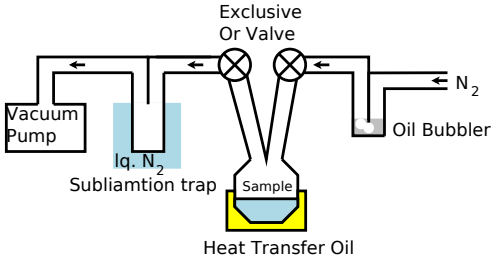
Water in air will evaporate or condense depending on air humidity. This presents a big challenge to controlling milligrams of water. A 10ml test tube at 22 °C and 50% humidity will hold 0.08 mg of vapor. This means that 0.08mg water can evaporate from the sample to the test tube air. The sample with the least amount of water, had 0.6 mg giving a minimum uncertainty of 13%. This also means that the air around an open test tube would have enough water to contaminate any of the samples.

## 5.1 Drying

One of the biggest challenges in this project was controlling the water content of the samples. Both the polymer and the salt are hygroscopic. Whenever the samples are exposed to air the dried samples will pick up water. The purchased chemicals may also contain water that needed to be removed at the start. The common practice for drying PPG is freeze drying.[9]. Several methods were used to overcome this problem. All glassware was dried in a vacuum oven before use. For storing prepared samples, glass test tubes with plastic screw lid were used. The lid was then sealed with Parafilm elastic film. For longer storage the tubes were stored in a desiccator. Drying the substances was first tried in a vacuum oven. However this method exposes the sample to air after drying.

The drying was instead done with a vacuum line shown in Figure 9. The vacuum line enables flasks to be closed with dry nitrogen inside them. The flasks are then transferred to glovebox atmosphere and opened. A dry nitrogen atmosphere is preserved throughout the process. The vacuum line consists of glass tube that connects a container to vacuum or nitrogen. It has a valve that can opened to apply either the vacuum or nitrogen. Routing the nitrogen trough a silicon oil bubbler acts as a one way valve. A liquid nitrogen cold trap is placed between the line and the vacuum pump, trapping any moisture. Moist air flowing into the cold trap will cool down and sublimate forming a ring of ice on the inside of the cold trap. The vacuum was obtained using an oil vacuum pump. The setup, including glass balloons, was dried using vacuum for an hour, to purge the system.

A magnet was used to stir both the polymer and the salt while drying. Crushing the crystals into a powder speeds up the drying. Two cycles of 2h vacuum followed by 30 min of $N_2$ at 80 °C were done. The cold trap was then removed and cleaned and a cycle was made to see if a ice ring forms again inside the cold trap.



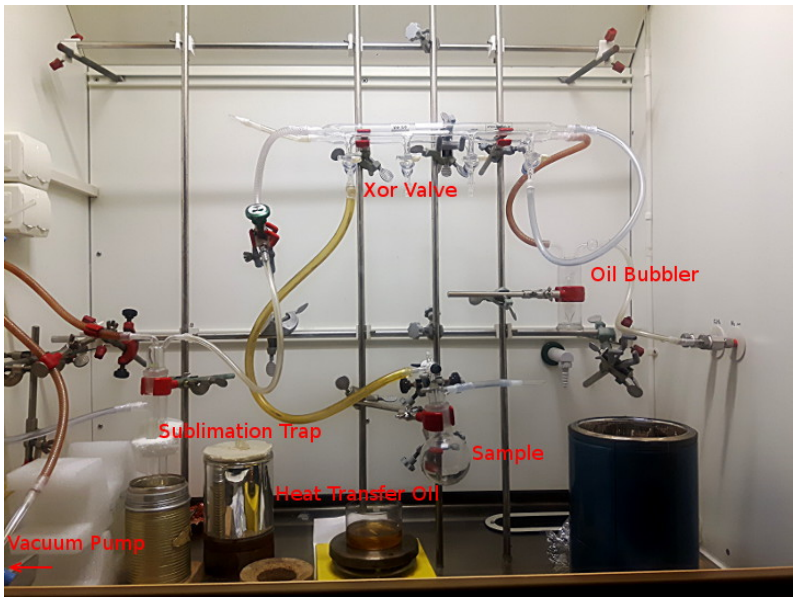




Figure 9: Vacuum line has tubes connected to vacuum and dry nitrogen atmosphere. The valve opens to either vacuum, dry nitrogen or is closed.

## 5.2 Sample Preparation

The samples were prepared in a glove box, pictured in Figure10. The atmosphere was purged with nitrogen gas. A beaker with silica gel was placed in the glove box to keep it dry when the nitrogen supply was off.

The LiTf was added to PPG in a test tube. When the test tube had been closed and sealed with 'parafilm' elastic film it was moved outside of the glove box. The sample was then stirred for at least 6 h at room temperature. Samples with 1.3 mol/kg LiTf or more were stirred at 100 °C , decreasing the viscosity enough to make it possible to stir.

Water was added to PPG4000-LiTf using three methods. All methods used a precision scale to weigh the sample before and after adding water.




Figure 10: Glove box used to prepare the samples under a nitrogen atmosphere. A small scale was used add desired weight of LiTf.

The first one was to add a drop of water to an empty tube in air. The tube was then sealed with elastic film and the PPG4000-LiTf was added in the glove box. The second method was to place a sealed off pipette with a drop of water in the glovebox. The water was then dripped into the tube of PPG4000-LiTf and then the tube is closed. The third method was to add water quickly in open air. The drawback with the first method is that the drop will start to evaporate before the lid is closed, and thus decreasing the measured weight of water. Moisture from the lab air can also get into the tube while it is open. Adding water in the glovebox has the drawback that it contaminates the glovebox atmosphere. This was measured using a hygrometer inside the glovebox. After the first samples were produced the evaporation was measured with IR. (Compare with the results in section 7.4.) A rough estimate of which samples would evaporate water could me made. This information was used to update the method. Samples with more water in them than the room air equilibrium used the third method of adding water in open air. After water was added the sample was stirred again at room temperature or on a 100 °C hotplate if too viscous. A picture of a sample with water added but not completely stirred can be seen in Figure11. Part of the sample has higher water content and is phase separated and appear milky, but the other is not and is transparent.



Figure 11: The picture shows a sample with a water drop added to the left side of the tube. The higher water content in that part means that it is phase separated and milky. The right part isn't. This shows the clear visual difference with phase separated samples.

## 5.3 Fourier Transform Infrared Spectroscopy

Infrared spectroscopy measures the absorbance through a large part of the infrared spectrum. Many chemical bonds have resonances in this frequency range, and can be analyzed by the total spectrum. The most straightforward way to do this is a monochrome IR light shone though a sample with the relative intensity being the amplitude at that point. Transmission requires that the sample is thick enough that some light is absorbed but not so thick that most light is absorbed. Total wave reflection has a electromagnetic amplitude a small distance inside the reflected material, called attenuation. Attenuated total reflection (ATR) was used by this project as an alternative to transmission. Figure 12 shows the difference between ATR and transmission.

ATR has the benefit of being independent of sample thickness. Modern IR spectrometers use a broad spectrum IR source to measure the many frequencies simultaneously. The IR source is a black body with a known spectrum. A fourier transform IR spectrometer will have the broad spec-

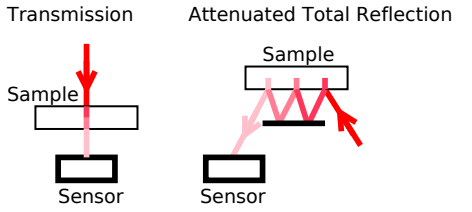



Figure 12: difference between attenuated total reflection and transmission infrared spectroscopy

trum IR pass through an interferometer, giving destructive and constructive interference according to the path length and IR wavelengths. A model of this can be seen in Figure 13 Next to it, a visible light laser interferometer will measure the path length. The interfered IR will then reflect against the sample and the total amplitude be measured. The amplitude at certain path length will be the sum of interference for all wavelenghts. The amplitude for the wavelenghts can be obtained by taking the fast fourier transform (FFT) of the amplitude for the path lengths.[14]

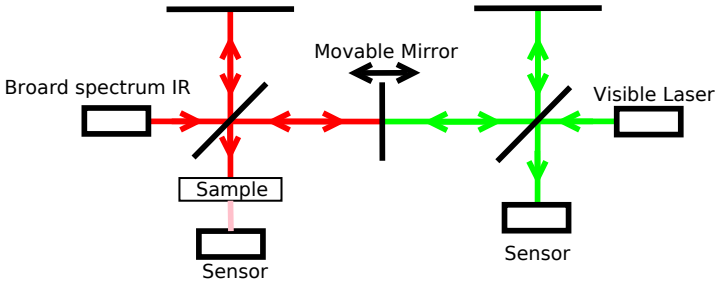



Figure 13: A simple model for a fourier transform IR spectrometer.

The spectrometer used was a Bruker alpha FTIR, with a range of 5000 $cm^{-1}$ to 400 $cm^{-1}$. The germanium plate limits the range to 5000 $cm^{-1}$ to 500 $cm^{-1}$. The samples were placed on the ATR plate in open air. A cover was placed over the sample drop to limit water evaporation and absorption. By placing a drop of water under the lid, the sample drop would absorb water to its 100% humidity equilibrium. By instead placing dry silica gel under the cover the sample could be dried to under 1% water, possibly <<1% using the method in section 7.4. The pure LiTf dissolved in water could be dried to negligible

water content and recrystallized. The crystals form on the ATR plate. All IR measurements were done at room temperature.

## 5.4 Thermogravimetric analysis

Thermogravimetric analysis (TG) uses a precision scale to measure weight changes in a sample. The sample is placed in a scale in glass chamber with a heater. A purging gas gives a constant atmosphere around the sample. By increasing the temperature linearly, compounds with a lower boiling temperature will evaporate earlier, until they are depleted. The compounds can then be identified by their boiling temperature. The mass evaporated in each step tells the amount of each substance. Thermogravimetry by its own can be ambiguous when two compounds have similar boiling temperature. The specific model used was Perkin-Elmer TGS-2 Thermogravimetric System.

## 5.5 Impedance Spectroscopy

Impedance spectroscopy has an advantage in that it can measure over several orders of magnitude, both in resistance and frequency. The low resistance of the setup compared to that of the electrolyte samples gives great accuracy. The impedance meter used, Agilent E4980A LCR-meter, has a range from 20 Hz to 2 MHz. The sample holder, shown in Figure 14, could hold liquid samples of varying thickness. The mixed sample was pippeted or smeared to the electrode. the upper electrode was then attached, while avoiding bubbles forming.

A moderate potential between an ionic solution and a blocking electrode will not conduct electrons. Instead ions or polarized molecules will build up a charge opposite to the charge of the electrons in the electrode. This is called an electrode double layer and will behave like a capacitor.[12] If the electrode is found empirically to be semi-blocking it can be modeled with a non-ideal capacitor. [9]

The setup couldn't measure the ionic conductivity directly so a model was made. The conductivity at the electrode-sample interface is mainly capacative, modeled as a capacitance, $C_i$. The conductivity of bulk sample comes from charge moving from the high voltage side to the low voltage side. There are two kinds of charge carries in the sample: free ions and dipoles. The ionic mobility will have a resistance. This ionic resistance is modeled as a resistance component, $R_b$. The dipoles tendency to align with the electric field is gives the permittivity. This permittivity is modeled as a capacitance, $C_b$. Because these conduction methods can occur in parallel, they are modeled as components in parallel.

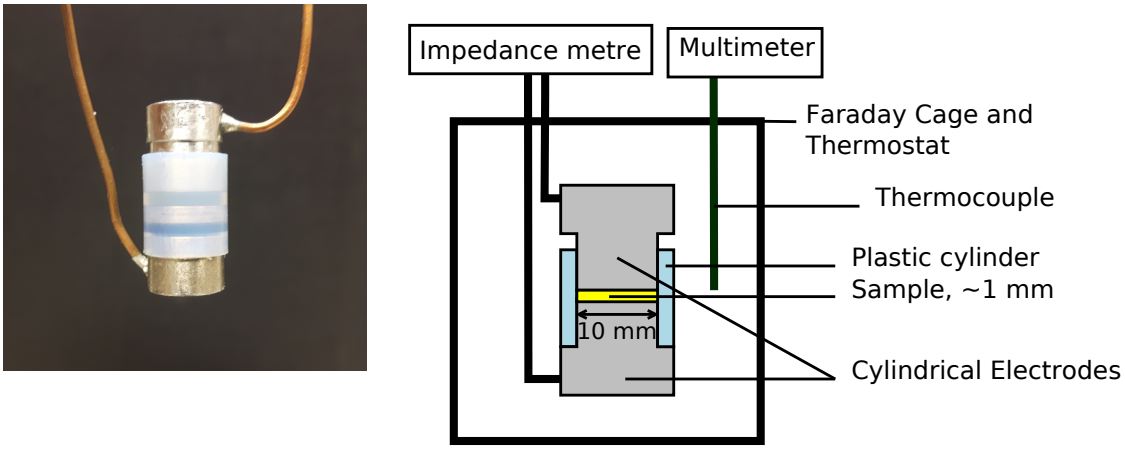



Figure 14: The impedance measuring setup.

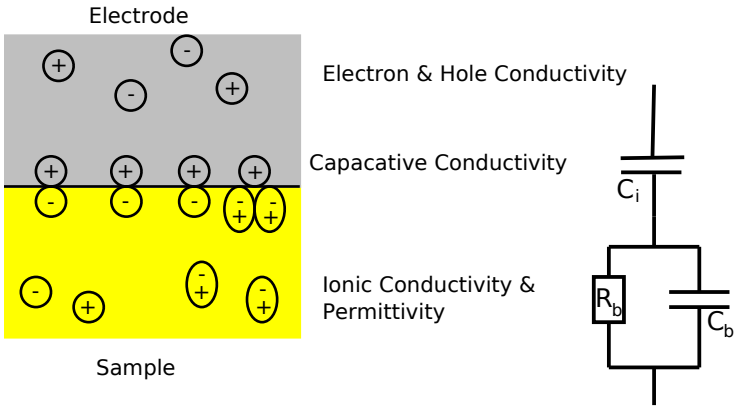



Figure 15: A zoomed in picture of the interface between electrode and the sample. The interface is modeled as a capacitance, $C_i$, and the bulk and a resistance, $R_b$, and a capacitance, $C_b$, in parallel.

The results in Figure35 show that the low frequency points have higher real impedance than the bulk resistance. A capacitance has purely imaginary impedance. This must mean that the interface impedance has resistive properties, that cannot come from a pure capacitance. The conductivity at the electrode-sample-interface is therefore modeled with a capacitance and a large frequency dependent impedance $Z_i(\omega)$ in parallel. The resistance is a model and should not be interpreted as physical conduction of electrons in the electrolyte. The setup has two electrode sample interfaces but they are

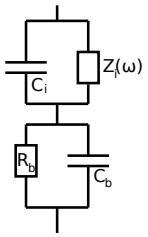



Figure 16: A equivalent circuit model with a more complex interface. The semi-blocking impedance $Z_i(\omega)$ is assumed to be very big.

symmetric, so their resistances can be added in the equivalent circuit model.

$$Z(\omega) = \frac{1}{1/Z_i(\omega) + \mathrm{i}C_i\omega} + \frac{1}{1/R_b + \mathrm{i}C_i\omega}$$

If one assumes $|Z_i(\omega)| > R_b$ and $1/R_b^2 >> C_i^2\omega^2$ then the imaginary part has a maximum at $\omega_2 = \frac{1}{R\sqrt{C_d C_i}}$ shown in Appendix A.1. This result doesn't contradict our assumption. Figure 17 show a Nyquist plot of the model system.

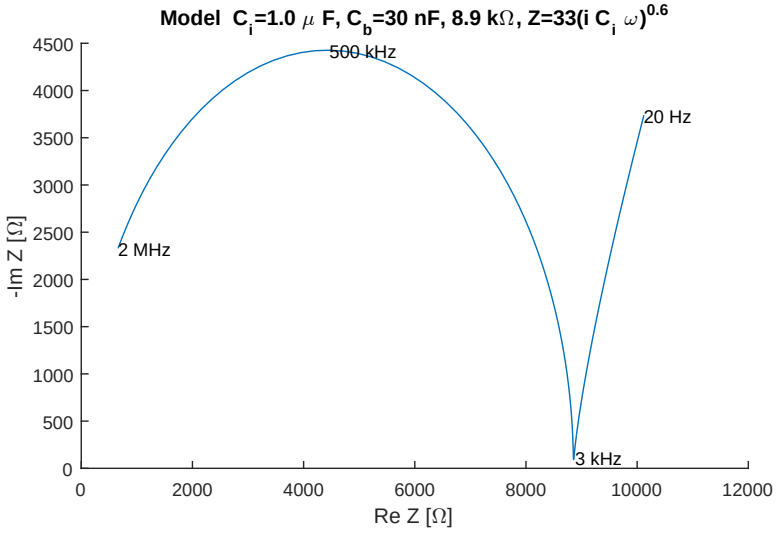



Figure 17: Nyquist plot of the model system.

It then follows that $Z(\omega_1) = R$, further

$$C_b = \frac{1}{R_b\omega_+}\sqrt{\frac{R_b}{\mathfrak{Re}Z(\omega_+)} - 1} \tag{4}$$

$C_i$ is the interface capacitance, $R$ is the Resistance from the ionic conductivity and $C_b$ is the dielectric conductivity. An ansatz for the semiblocking, $Z_i(\omega)$, would be $a(iC_i\omega)^b$ where $a >> 1$ and $0 < b < 1$.

$$\sigma = \frac{d}{A * R_b}$$

The permittivty $\epsilon$ of the sample is found by canceling the conductivity. Some authors use the relative permittivity is $\epsilon = \epsilon_0\epsilon_r$. In this simplified model the $C_b$ is a direct consequence of the permittivity of the sample. This can be used to find the permittivty of the samples. If the geometry of the sample is simple then,

$$\frac{dC_d}{A} = \varepsilon$$

An alternative method to find the permittivity is the calculate the *frequency dependent complex permittivity*. If the geometry of the sample is simple then,

$$\frac{d}{\mathrm{i}\omega * AZ} = \hat{\varepsilon}$$

The plateau of the real part complex permittivty is the *permittivity value*[9]. The permittivity value is the actual polarization ability of a medium.

Lets consider a simple circuit.

$$Z(\omega) = \frac{1}{1/R + \mathrm{i}C_b\omega}$$

The complex permittivity would be

$$\frac{d}{\mathrm{i}\omega * A\frac{1}{1/R+\mathrm{i}C_b\omega}} = \hat{\varepsilon}$$

$$\frac{d}{\omega * A}(-\mathrm{i}/R + C_b\omega) = \hat{\varepsilon}$$

And real part complex permittivty $\mathfrak{Re}\hat{\varepsilon} = \varepsilon'$

$$\frac{d}{A}C_b = \varepsilon'$$

The model circuit from Figure 16 has the impedance:

$$Z(\omega) = \frac{1}{1/Z_i(\omega) + \mathrm{i}C_i\omega} + \frac{1}{1/R_b + \mathrm{i}C_i\omega}$$

The theoretical model circuit permittivity value is $dC_b/A$. This makes it interesting to compare with its frequency dependent complex permittivity shown in Figure 18. The value of the plateau is used to find the permittivity for unknown circuits. For this model circuit the value of the plateau $11\varepsilon_0$ is exactly the same as the theoretical $dC_b/A$, but might differ for real samples.

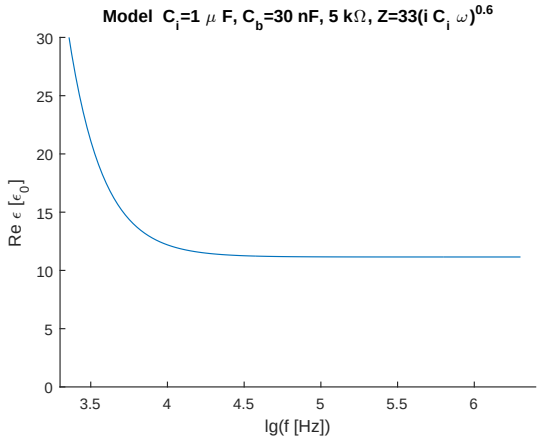



Figure 18: The equivalent circuit model is used as an example of the frequency dependent complex permittivity. The value of the plateau is $11\varepsilon_0$. The Y axis is the real part of the complex permittivity. $d$ is 0.26 mm and the $A$ is 83 mm$^2$

# 6 Experiment

The air in the lab has a temperature of 21 °C and a relative humidity of approximately 50%. The humidity could vary between 30% to 80% depending on the weather. LiTf concentrations of between 0.084 and 2.7 mol/kg were produced. The samples with high LiTf concentrations were increasingly viscous. The 2.7 mol/kg LiTf sample would hold its shape for hours. The viscosity was not measured quantitatively. The prepared samples had water content between 0.1% to 25%. Tables 6 and 7 show the comparison between molality and weight fraction as well as molecule ratios. The ratio of 64 repeating units to end groups means that the proportion of endgroups OH to water goes from 1:2 to 1:69.

The method for adding water was hard to verify. There where sources of moisture contaminants. Repeated opening of the sluice resulted in a relative

Table 6: LiTf — PPG4000 concentrations of investigated samples.

| LiTf weight fraction | Molality [mol/kg] | #PPG4000 (rep):#LiTf | #OH:#LiTf |
|---|---|---|---|
| 1.3% | 0.084 | 204:1 | 6:1 |
| 4 % | 0.27 | 64:1 | 2:1 |
| 9 % | 0.63 | 27:1 | 1:1 |
| 17 % | 1.3 | 13:1 | 1:2 |
| 30 % | 2.7 | 6:1 | 1:6 |

Table 7: PPG4000 — water concentrations of investigated samples.

| Water weight fraction | Molality [mole/kg] | #PPG:#Water |
|---|---|---|
| 1.3 % | 0.73 | 24:1 |
| 3 % | 1.7 | 10:1 |
| 9 % | 5.5 | 3:1 |
| 17 % | 11 | 3:2 |
| 25 % | 18 | 1:1 |

humidity of 15%. The samples where in equilibrium with the atmosphere in the test tube. When the tube was opened, it was generally not in humidity equilibrium with the outside air. This means that with every opening up to 0.08mg of water could be lost or gained. This uncertainty is not large enough to explain the variation in conductivity for similar samples. The conductivity outliers could be from incorrectly measured thickness or incorrect water content.

The impedance meter could find the conductivity but could not measure the permittivity of all samples. Conductivity peaked at around 1 molality LiTf. Water was found to increase the conductivity, but the most for sample with either low or high LiTf concentration. Thermogravimetric analysis was not able to measure the water content with sufficient accuracy. Water had time to evaporate before the measurement started. The IR spectroscopy showed how the water content changed over time. Several bands in the 950 to 1350 $\mathrm{cm}^{-1}$ range were shifted in PPG4000-LiTf mixes. The 1042 $\mathrm{cm}^{-1}$ $SO_3$ stretch band shifted when water was added.

# 7 Results and Discussion

Due to the hygroscopic properties of LiTf, it was a challenge to keep the sample dry. The samples shad to be kept dry to preform measurements of their dry state. If the dry LiTf salt was left in open air for a minute, it would become wet and sticky. If left for a few more minutes it would absorb enough water to completely dissolve the LiTf in the water. For the IR spectroscopy the PPG4000-LiTf sample was in open air but by being quick (a few seconds), and putting a lid on the sample, the water content could be preserved enough for measurement. The preparation for the thermogravimetry took a few minutes and the original water content had changed by the time the experiment started. This was taken into consideration. The impedance cell was air tight and didn't have the same problem. The impedance cell was prepared in a glove box, preserving the dry samples. This means that the

water content for the impedance results are more reliable.

## 7.1 Thermogravimetric Measurements

Figure 19 shows thermogravimetric analysis of LiTf with water. A 1.3% mass loss between 30 °C and 45 °C is attributed to water evaporating. The graph with measured and set temperature show that the heating was linear in this range. A 18% mass loss between 60 °C and 100 °C is also attributed to water evaporating. The values comes from the size of the 'step' and are very approximate. LiTf decomposes around 500 °C, in two stages. This shows that the 80 °C used during the drying in the vacuum line was sufficient but on the low end.

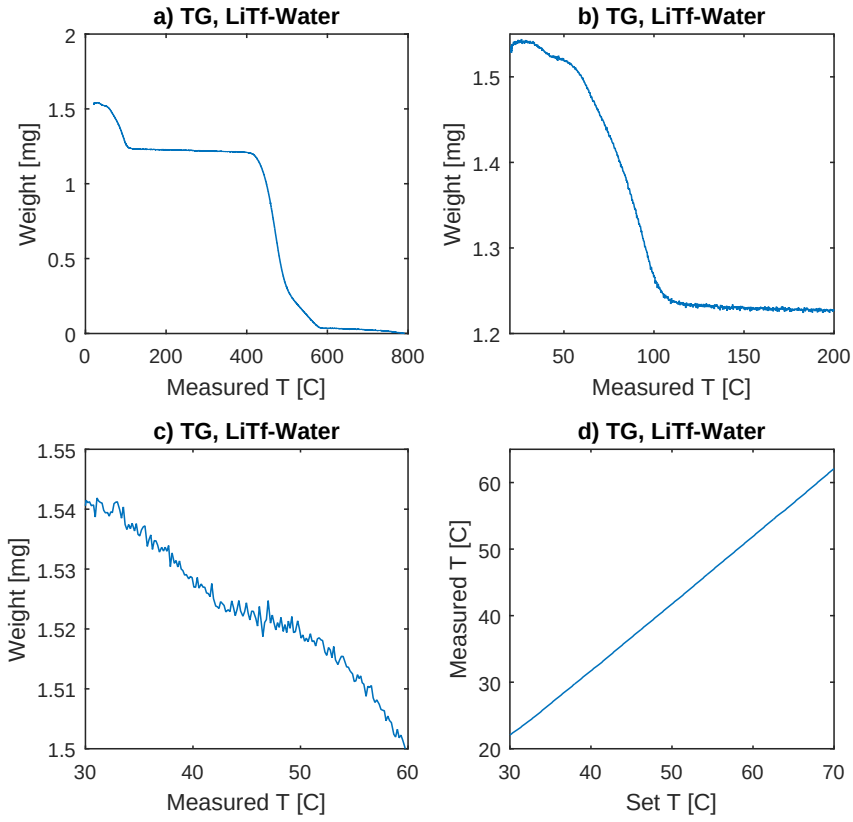



Figure 19: Thermogravimetry of LiTf with water. Subfigures (a-c) show different ranges of the same graph. Subfigure d) shows the difference between measured and set temperature to rule out heating rate errors. The water content at the start of the measurement was unknown.

The thermogravimetric analysis of PPG4000 in Figure 20 shows a slight

inflection point around 80 °C. It would correspond to 0.05 mg out of 15 mg. This corresponds to a weight ratio of 0.3%. This is not unreasonable for the water content. The initial water content is deduced using the results in chapter 7.4. It did also show that the polymer decomposed at 360 °C .

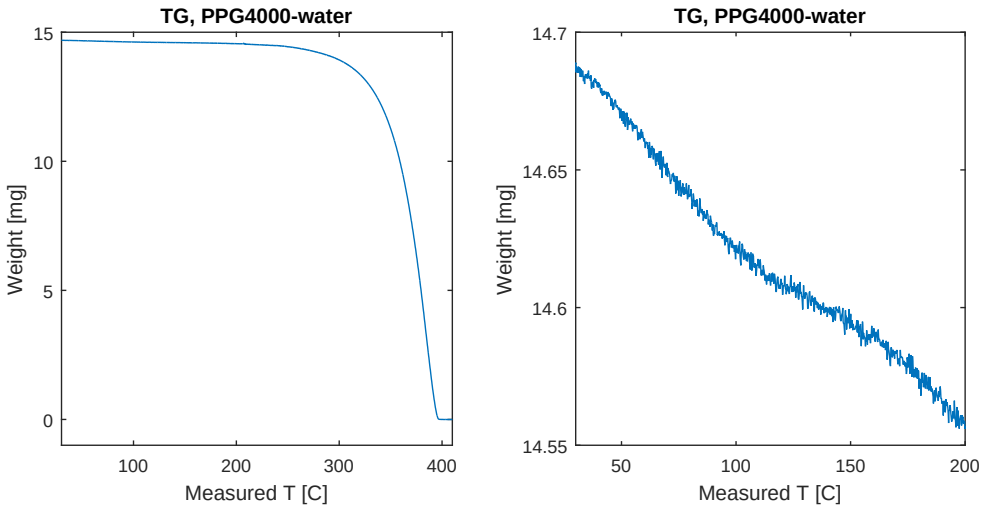



Figure 20: Thermogravimetry analysis of PPG4000. It reached water equilibrium with air before the experiment. The plots show different interval of the same graph. A slight inflection point can be seen at 80 °C.

Thermogravimetric analysis of PPG4000-LiTf in Figure 21 shows that there is a smooth mass loss accelerating into decomposition. The PPG4000-LiTf decomposes at approx 370 °C. It showed that the water content was low. The decomposition of PPG4000 is confirmed by Figure 22, showing a different concentration.

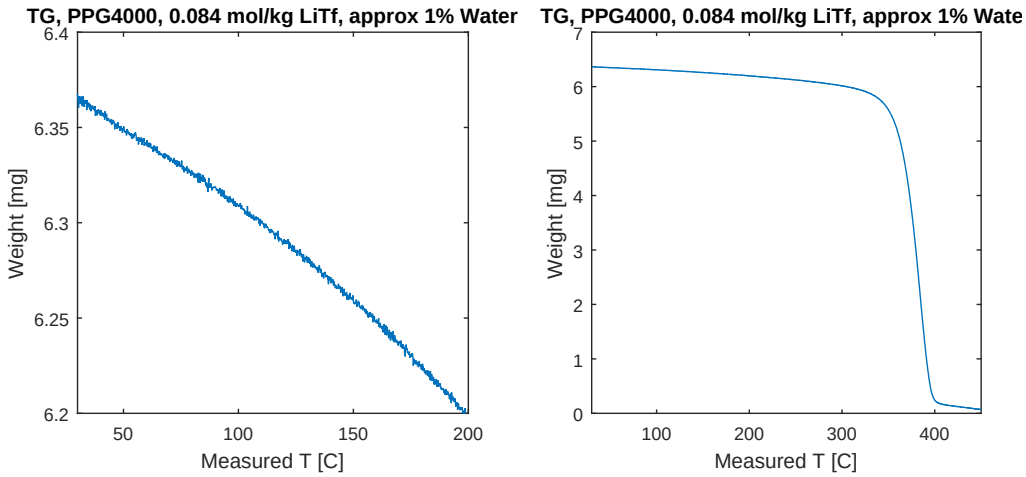



Figure 21: Thermogravimetric analysis of PPG4000 complexed with 0.084 mol/kg LiTf. It reached water equilibrium with air before the experiment. The start water content was approximately 1%.

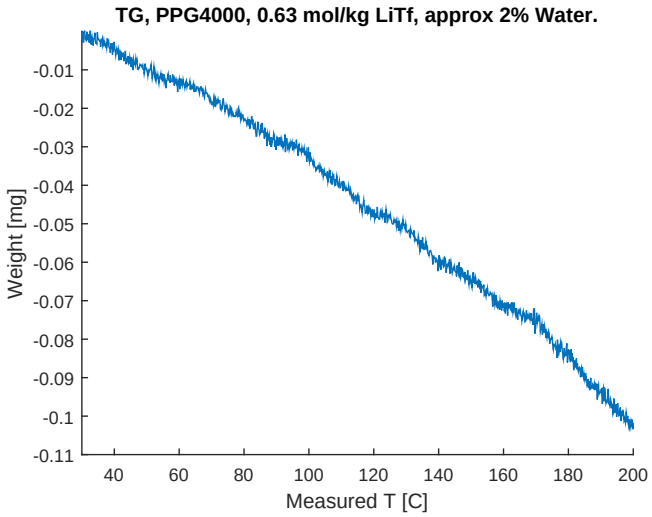



Figure 22: Thermogravimetry analysis of PPG4000 complexed with 0.63 mol/kg LiTf. It reached water equilibrium with air before the experiment. The start water content was approximately 2%. The Y axis shows mass difference.

## 7.2 IR spectrum of PPG4000-Water

The IR spectrum of PPG4000-water in Figure 23 shows the $CH_x$ stretching bands between 2800 $cm^{-1}$ and 3000 $cm^{-1}$. The CO stretching and $CH_x$ bending bands are between 800 $cm^{-1}$ and 1500 $cm^{-1}$. The PPG4000 OH band is between 3300 $cm^{-1}$ and 3600 $cm^{-1}$. The water OH band is between 3100 $cm^{-1}$ and 3700 $cm^{-1}$. The pure water OH band is also between 3100 $cm^{-1}$ and 3700 $cm^{-1}$. The PPG4000 CO or $CH_x$ bands doesn't overlap with the water OH bands. The untreated PPG4000 had a water content of <0.035% according to the manufacturer. The water content could only be verified to be below 1% using IR. It was observed that excess water evaporates to below 1% within minutes. This was measured with the method described in 7.4.

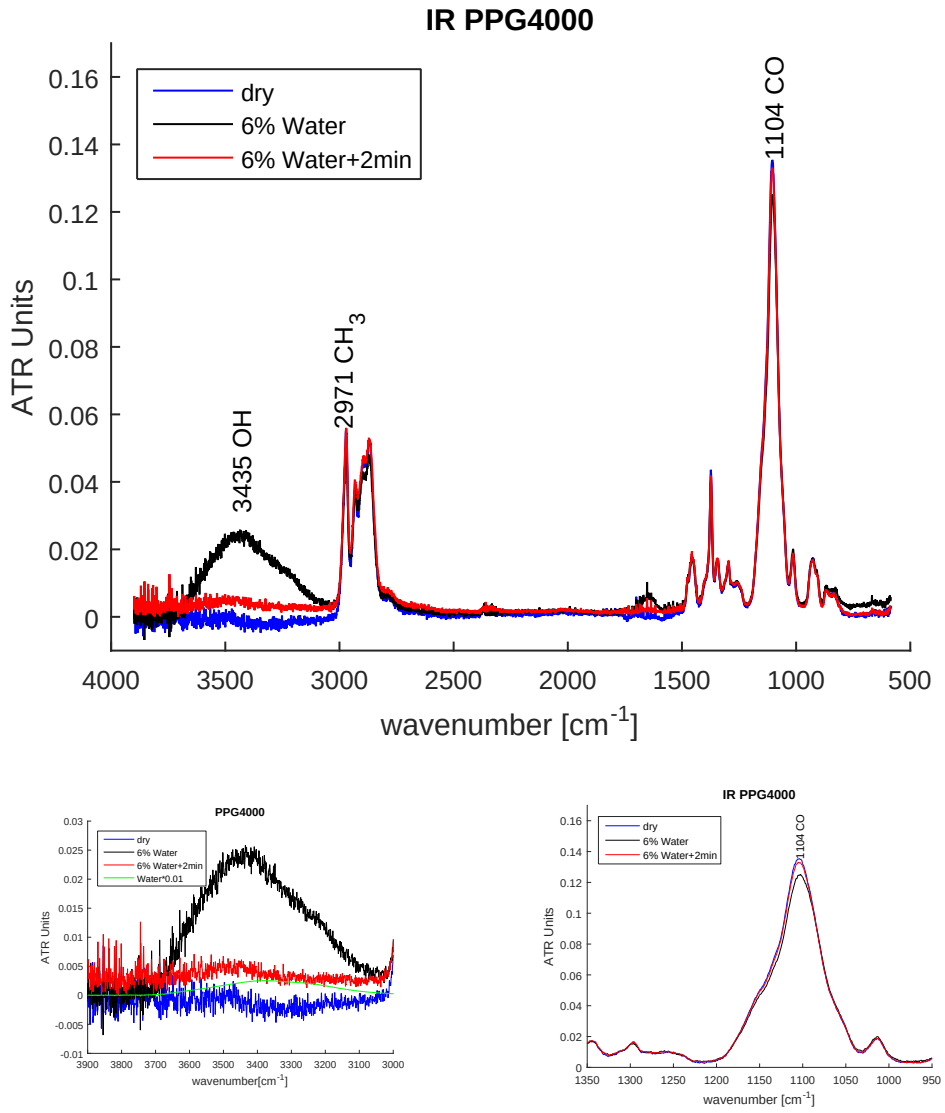



Figure 23: IR spectrum of PPG4000 with different concentrations of water. The 6% water sample is phase separated. The plots show different ranges of the same graphs.

## 7.3 IR spectrum of Lithium Triflate-Water

LiTf is crystalline when dry. It absorbs water from air to form drops of 33% water and 67% LiTf, completely dissolving the LiTf in the water. The IR spectrum in Figure 24 of LiTf has bands. The water OH-stretching band is shifted to 3525 $\mathrm{cm}^{-1}$. The bands that are change the most the most 1289 $\mathrm{cm}^{-1}$

and 1222 $cm^{-1}$ . The 1289 $cm^{-1}$ band is $SO_3$ stretching, and this means that $SO_3$ interact with the water.

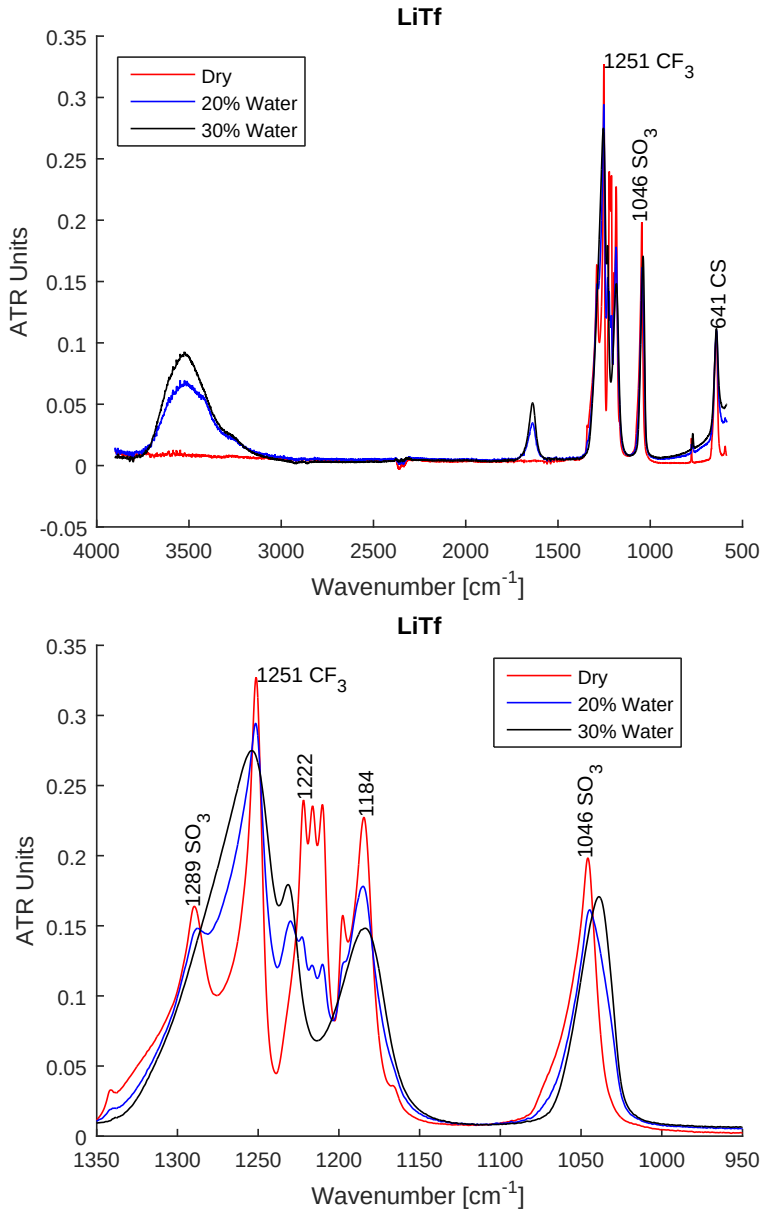



Figure 24: IR spectrum of LiTf with water. The LiTf was dried using silica gel. The water bands is similar to that of pure water but the LiTf bands is very different in the 950-1350 $cm^{-1}$ range. IR spectrum of LiTf shows $SO_3$, $CF_3$ and SC bands. Hydration affects the 1289 $cm^{-1}$ and 1222 $cm^{-1}$ bands the most.

## 7.4 PPG4000-LiTf-Water Equilibrium with Air

Water has a big, very broad band at 3375 $cm^{-1}$ and a smaller at 1640 $cm^{-1}$. The PPG4000-LiTf-water evaporate water over time. An example of this is in Figure 25. It can also be seen that the OH band is 3400 $cm^{-1}$ for 1.5% water sample, at 3500 $cm^{-1}$ for the 10% water sample. The dry sample absorbs water and the wet samples evaporates water. Both the wet and dry sample approach an equilibrium within hours. By comparing with pure water, an approximate concentration of water can be deduced. We know from Table 1 that PPG4000 has the same density as water. We know from Figure 23 that the PPG4000-water spectrum is close to a linear combination of the two.The PPG4000 CO IR band at 1103 $cm^{-1}$ is not shifted in the presence of water. A strong interaction between water and the PPG4000 chain would be expected to shift this band. This reinforces the hypothesis that water mostly interacts with PPG4000 endgroups.

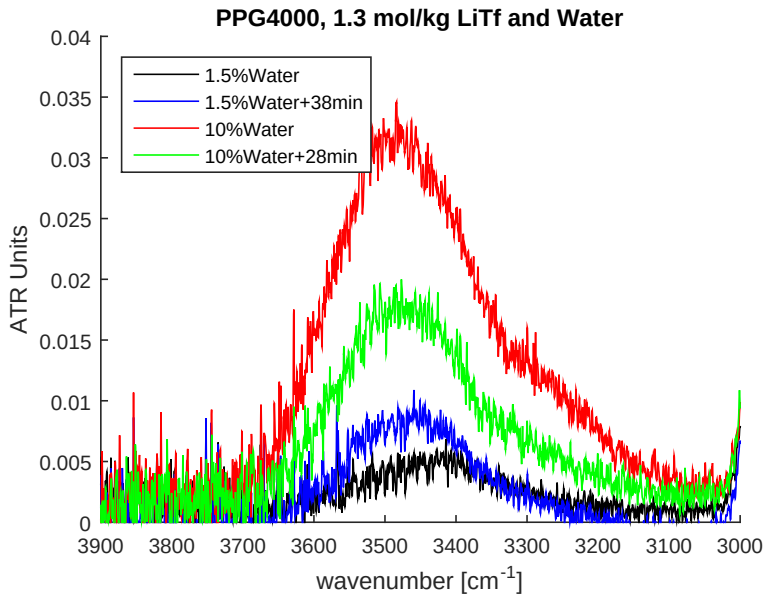



Figure 25: The dry sample absorbs water and the wet sample evaporates water. Both the wet and dry sample approach an equilibrium within hours. The dry sample was initially dry (<<1% water) but had absorbed approximately 1.5% water by the time the experiment had started.

## 7.5 Phase Separation of PPG4000-LiTf-Water

Some of the samples showed phase separation. This was identified visually. The picture in Figure 26 shows a sample where one half is phase separated and the other part is homogeneous and transparent. The phase separation used data from the IR measurements described in 7.4. Figure 26 shows both the approximate water equilibrium points and what water concentrations yielded phase separation. The phase separated samples didn't form layers because of gravity, suggesting the two phases ad very similar density. PPG4000 dissolve 4 % water before separating into a wet polymer phase and an aqueous phase. Mixing in LiTf increases the amount of water that can be dissolved to more than 20%. In open air PPG4000-LiTf mixes absorb or evaporate about a seventh of the maximum dissolved water. End groups are very important for the solubility of water in PPG4000. Phase separation occurs when the water content is high, and the PPG4000 is saturated. Since water doesn't dissolve pure PPG4000 the phases will be 96% PPG4000-4% water and 100% water. Figure 27 shows infrared spectrum of a macrophase separation. A drop of water was placed next to PPG4000-LiTf-water sample. The water attracted LiTf but very little PPG4000. The aqueous sample attracted a higher concentration of LiTf than the original sample. The rough proportions are shown in Figure 28. The the two composition are in equilibrium in the macrophase separation, they must also be in equilibrium in microphase separation. It is reasonable to assume that the microphase separation has the same composition, with a wet PPG4000 rich phase and an aqueous phase.

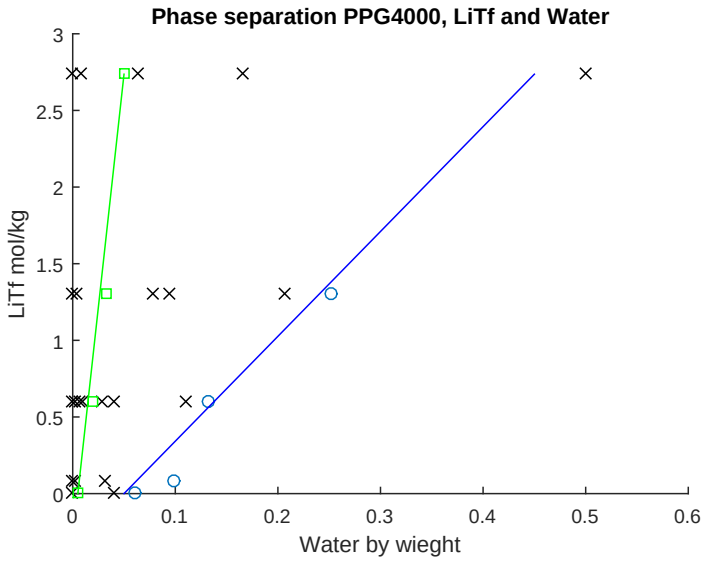



Figure 26: Plot of samples that phase separate. The black crosses are homogeneous samples and the blue rings a phase separated samples. The green squares show the equilibrium points with air. The lines are just a guide for the eye. The saltier samples require more water to phase separate.

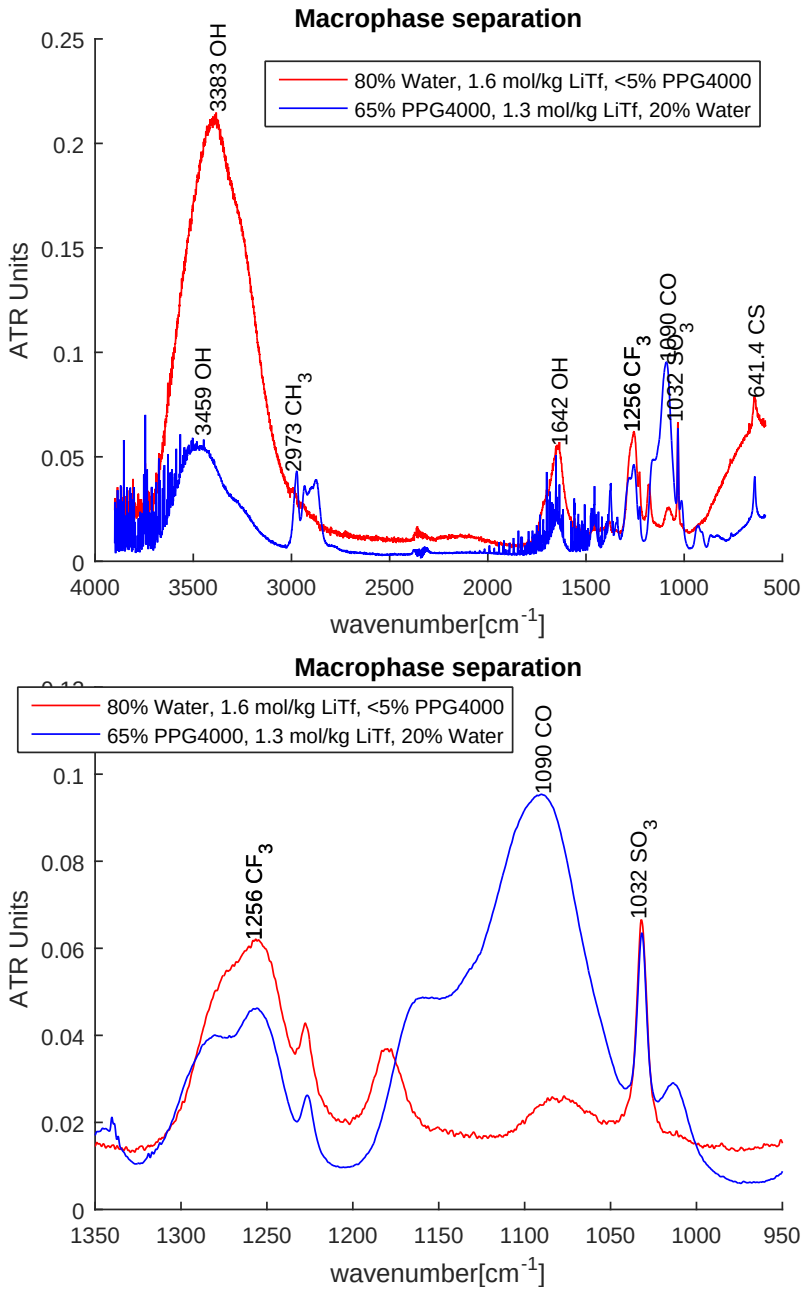



Figure 27: The blue line is a sample with PPG4000, LiTf and water. A drop of water was placed next to the blue sample, attracting LiTf, and was measured as the red line. The aqueous sample attracted a higher concentration of LiTf than the original sample. The aqueous sample showed weak PPG4000 bands.

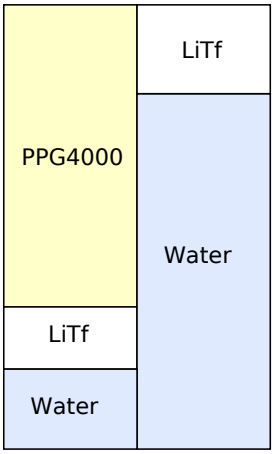



Figure 28: Diagram based on the situation in Figure 27 . One wet, PPG4000 rich phase, one aqueous phase with higher concentration of LiTf and possibly PPG4000. The physical appearance is like Figure 8.

## 7.6 IR spectrum of PPG4000-LiTf-Water

The IR spectrum in the 950-1350 $cm^{-1}$ range in Figure 29 is different for PPG4000-LiTf mixes than the components on their own. Figure 30 zooms in on this interesting region. The large PPG4000 C-O stretching band is the unaffected in the low LiTf samples. In the high LiTf concentrations, the C-O band is separated into two distinct bands. The pure PPG4000 1104 $cm^{-1}$ CO band is lower. This must correspond to an interaction with its environment. Both S-$O_3$ and C-$F_3$ asymmetric stretching bands are present. The symmetric S-$O_3$ stretching has two bands, but the higher wavenumbmer band is stronger. In the IR spectrum of PPG-LiTf-water mixes it is easy to separate the bands from water it self. The symmetric S-$O_3$ stretching has two bands and in the wet samples the low wavenumber 1031 $cm^{-1}$ band is stronger. The $SO_3$ stretch band is displayed in Figure 32.

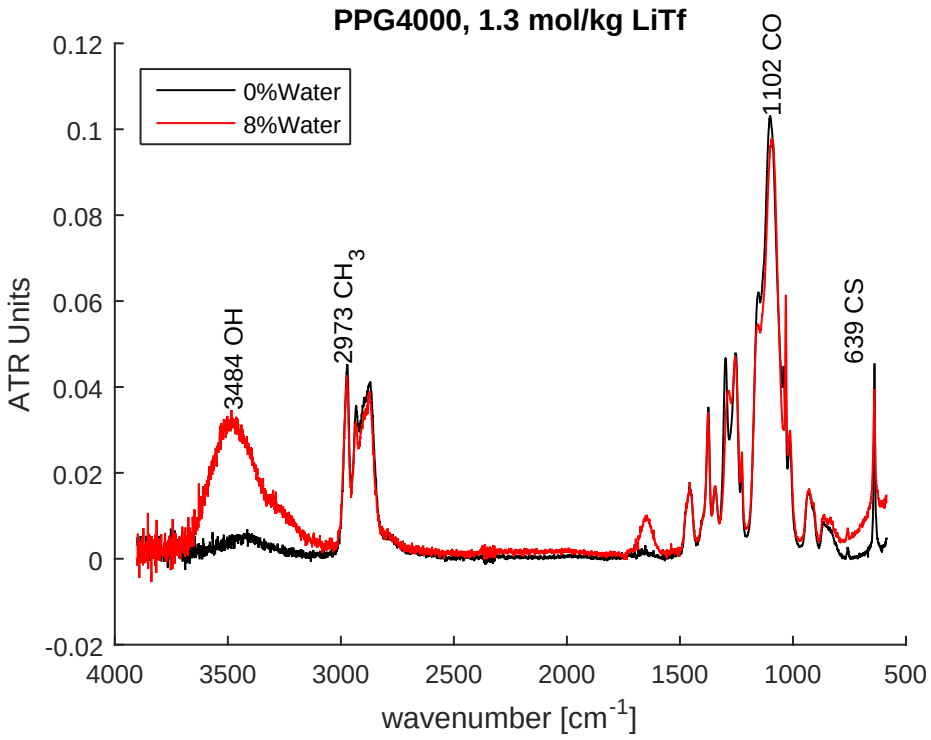



Figure 29: PPG4000 1.3 mol/kg LiTf. The water OH band if clearly visible in the 8% water sample. The bands in the 950-1350 $cm^{-1}$ range are different. The value 3484 $cm^{-1}$ for the OH band is very approximate.

.

The IR bands of LiTf dissolved in PPG4000 are very different from those in aqueous solution, especially $SO_3$. The PPG4000 CO band is attenuated

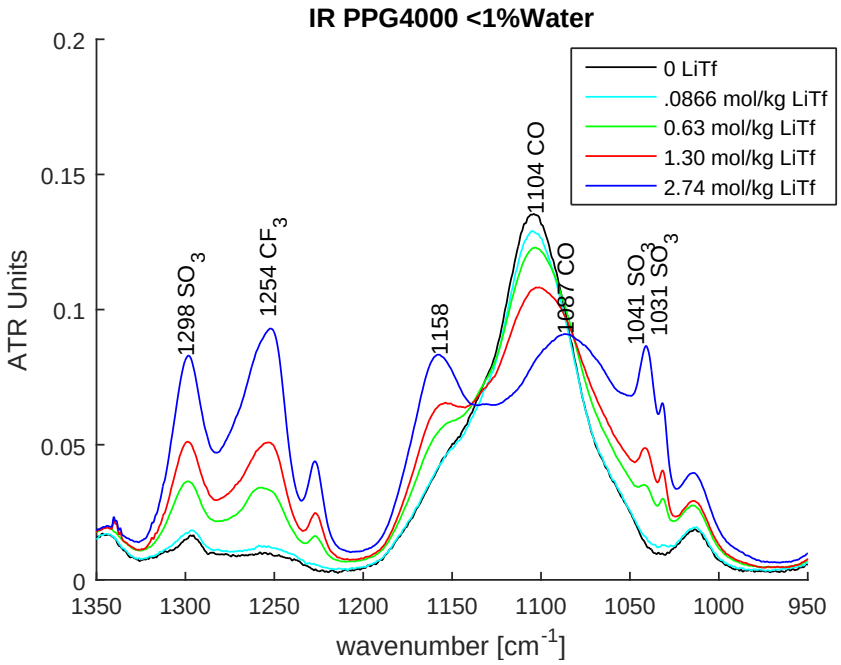



Figure 30: IR spectrum of PPG4000, LiTf. The LiTf bands are different in PPG4000 solution. $SO_3$ ,$CF_3$, symmetric and asymmetric stretching bands are visible. Note how the symmetric 1040 $cm^{-1}$ $SO_3$ stretching band is split in two. In the high LiTf concentration sample, the PPG4000 C-O band is redshifted. Note how the asymmetric 1289 $cm^{-1}$ $SO_3$ bands is weekend and redshifted in wet samples.

and split in two. LiTf enables more water to be mixed into the PPG4000 without phase separation. This suggests that LiTf interacts with both, and acts like a glue between the two. This is must correspond to LiTf interacting with both water and PPG, on a molecular level. This is confirmed by the PPG-LiTf-water IR spectra. Ferry and Tian[4], concludes that OH end group - salt interactions are important, even for PPG4000. They also conclude that PPG4000 and LiTf will form ion pairs and ion complexes, lowering the conductivity. Bishop et al.[5] uses the $SO_3$ stretch IR band to investigate ion association behavior. Adding N,N'-dimethylformamide was found to lower ion association. PPG-LiTf-water IR spectra has the $SO_3$ band split in two. One is stronger in dry samples, and the other in wet. These must correspond to two molecular interactions. For water the only candidate is OH - $SO_3$. In 2.74 mol/kg concentration the bands are equally strong when the ratio of water to LiTf is about 0.6 as seen in Figure 32 and 33. The other coordination must be to either PPG4000 or $Li^+$. This equilibrium $H_2O$

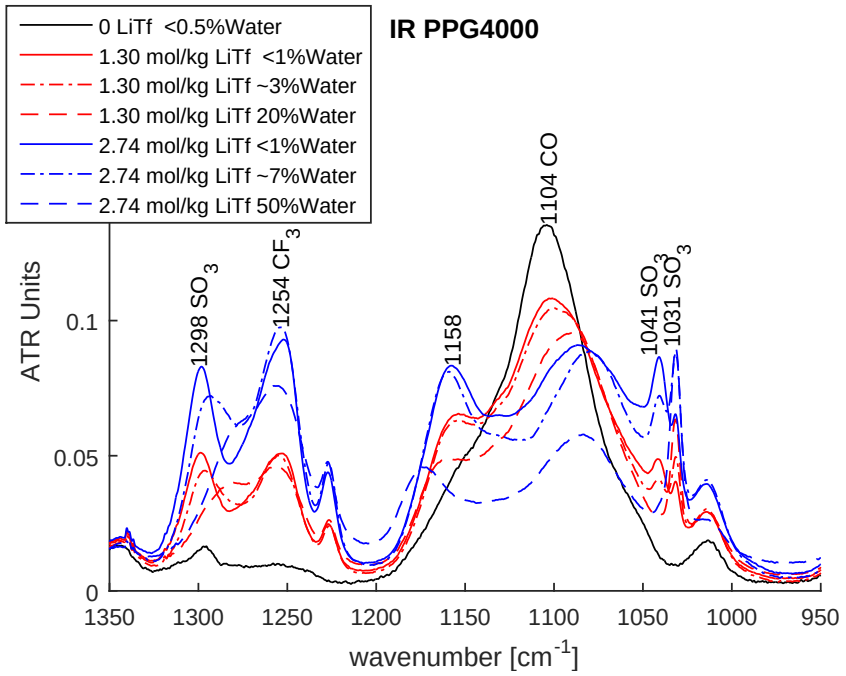



Figure 31: IR spectrum of PPG4000, LiTf and water mixes. Note how the symmetric $SO_3$ stretching band is split in two. In the high LiTf concentration sample, the PPG4000 C-O band is redshifted. Note how the asymmetric $SO_3$ bands is weekend and redshifted in wet samples. The split symmetric $SO_3$ stretching bands show that water intensifies the redshifted band and decreases the blueshifted.

- $SO_3$ ratio is independent of the LiTf concentration. Since $Li^+ = SO_3 \propto H_2O$ at equilibrium this can be stated as the other coordination is independent of the relative PPG4000 concentration. This makes $Li^+$ coordination a more likely candidate. This would mean that there are a large portion of ion pairs in all concentrations LiTf. Figure 30 shows that the $1041\,cm^{-1}$ $SO_3$ band is significantly stronger in the 2.7 mol/kg LiTf sample. Also in the 2.7 mol/kg LiTf sample the main CO band is weakened and instead the $1087\,cm^{-1}$ CO band is stronger. This can't com from CO - $SO_3$ interaction because of the $SO_3$ band. The only possibility is CO - $Li^+$ interaction. The CO bond is polar $C^{\delta+}O^{\delta-}$ and the the $Li^+$ will coordinate with the oxygen. For reference the 2.7 mol/kg LiTf sample had 6 oxygen for every $Li^+$. Figure 34 shows an overview of molecule interactions.

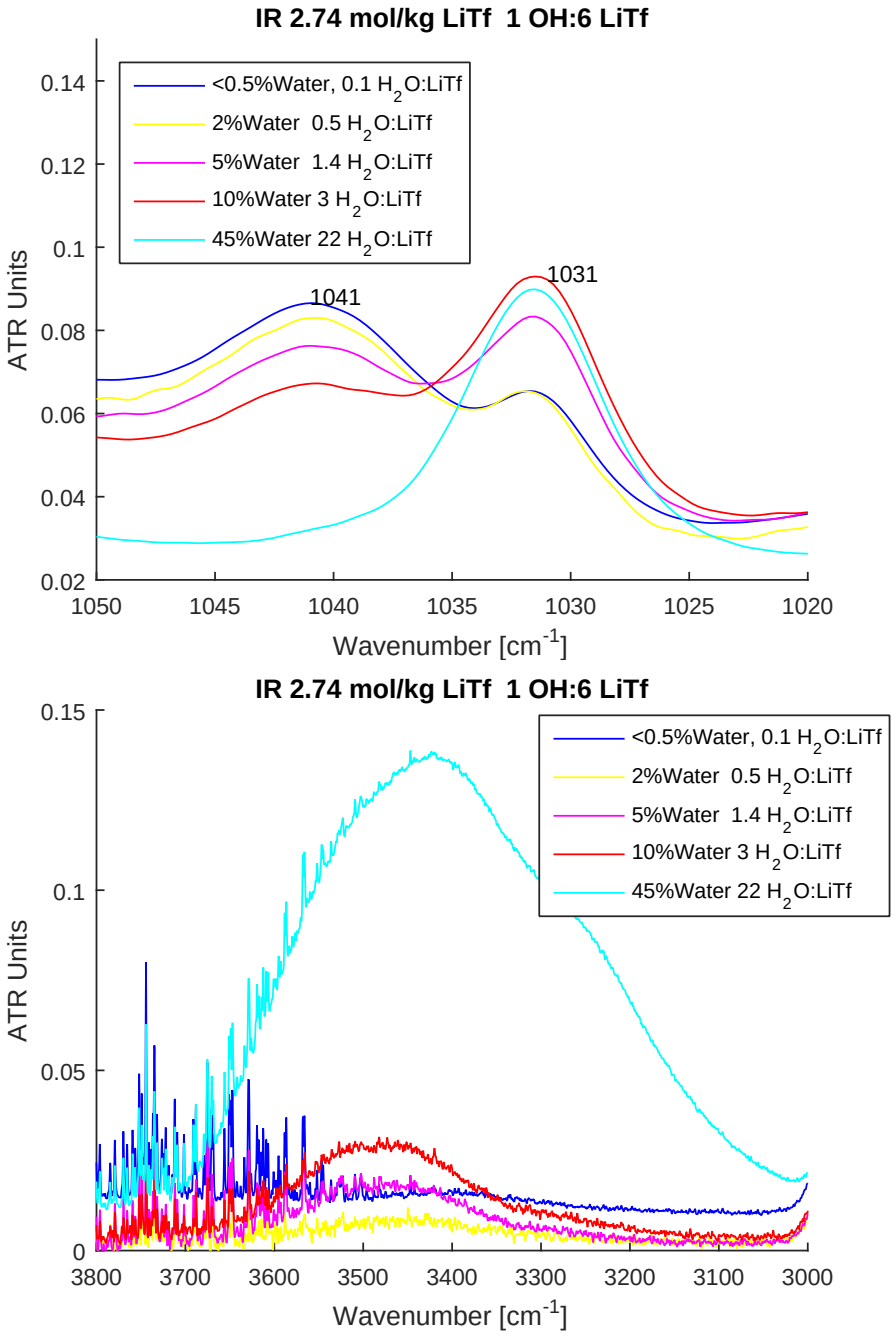



Figure 32: IR $SO_3$ stretch band of PPG4000, LiTf and water mixes. Water to LiTf molar proportions for comparison. The bands are equally strong when the ratio of water to LiTf is about 0.6. At these concentrations there are 6 or 27 monomers for every LiTf

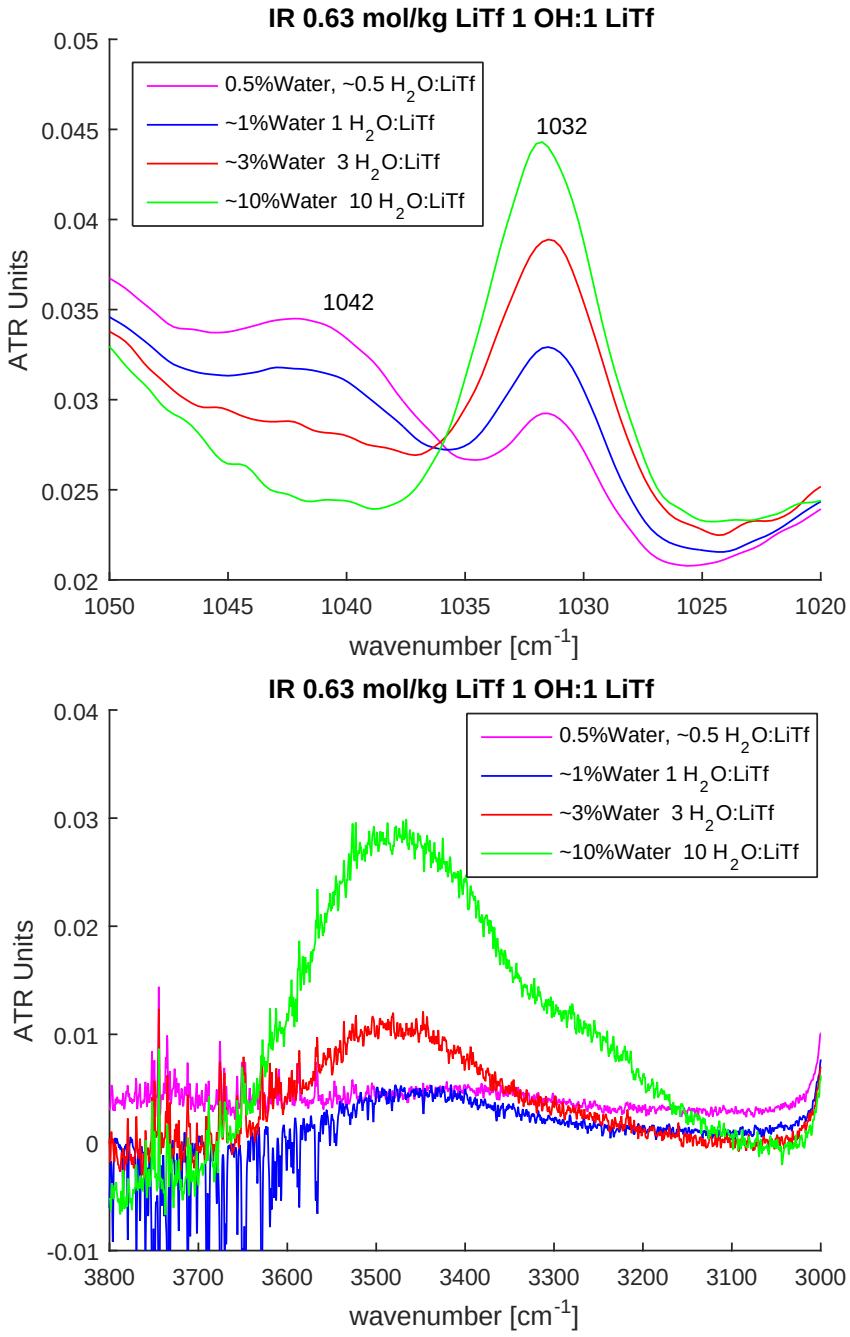



Figure 33: IR $SO_3$ stretch band of PPG4000, LiTf and water mixes. Water to LiTf molar proportions for comparison. The bands are equally strong when the ratio of water to LiTf is about 0.6. At these concentrations there are 6 or 27 monomers for every LiTf

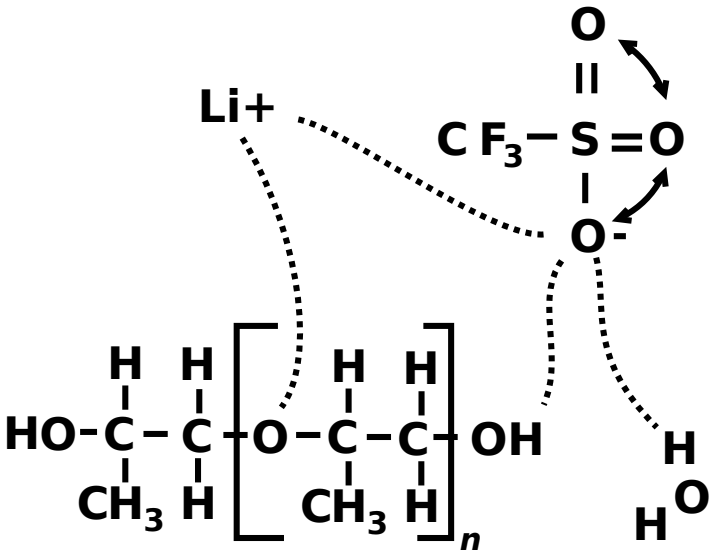



Figure 34: An overview of molecule interactions. $Li^+$ competes with OH to interact with $Tf^-$

## 7.7 Impedance Measurements

The sample bulk resistance was conclusive for all sample except the pure PPG4000, using the impedance data. Measuring the conductivity of pure PPG4000 should be seen as the limit of what is possible with this method. The impedance curves had very low noise making it an excellent tool to study the conductivity. Figure 35 shows the Nyquist plots for some samples ranging from low to high conductivity. The impedance of the samples spread through several orders of magnitude. In all samples the imaginary part of the impedance had a minimum. This imaginary impedance minimum was taken as the resistance as described in section 5. The fact that the imaginary part of impedance had clear minimums confirms the accuracy resistance points. The frequency increases from right to left. The left side semicircle, high frequency, is from sample permittivity. the right part, low frequency, comes from the interface impedance. Most samples had points with higher frequency then the frequency of the minimum imaginary impedance point. A point with higher frequency then the frequency of the minimum imaginary impedance point was used to fit the model. The model from section 5 is a good fit, but not

for dry PPG4000 or samples with more than 15% water. The permittivity could be calculated for most of the samples. The interface semi-blocking impedance is set to $Z_i(\omega) = 33(\mathrm{i}C_i\omega)^{-0.6}$ . The values in the semi-blocking impedance was found empirically.

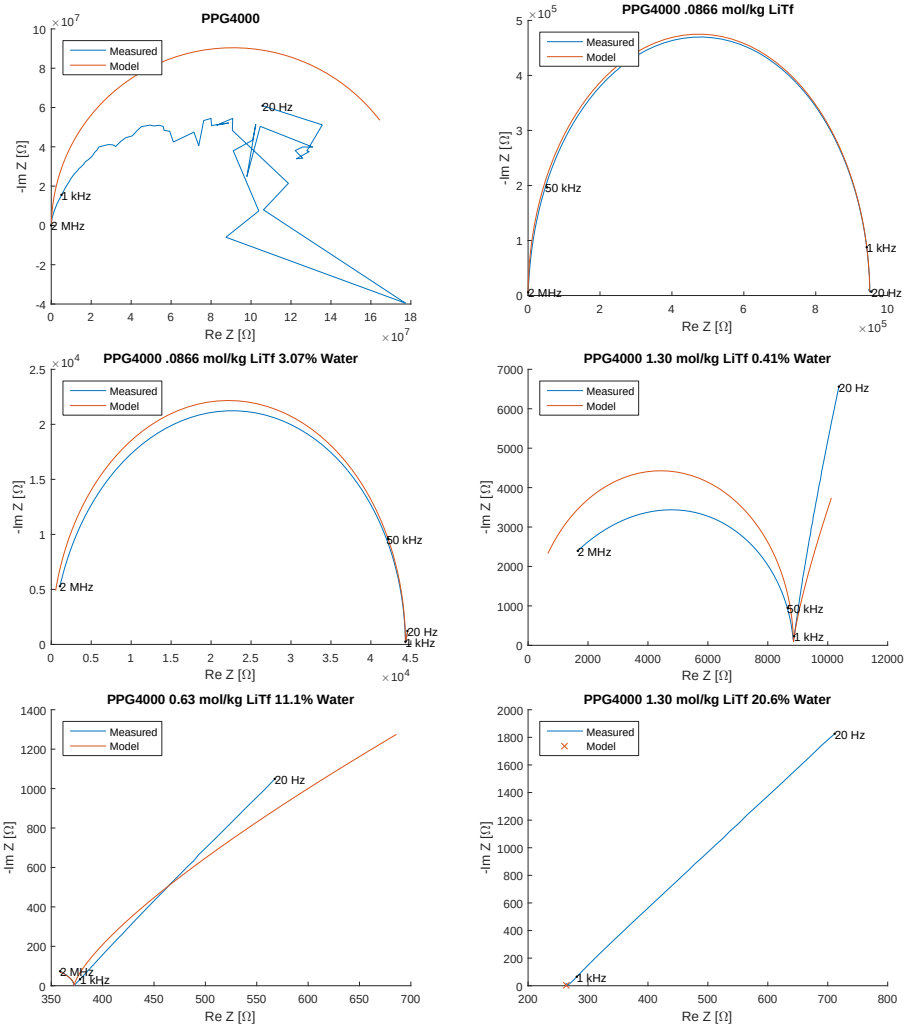



Figure 35: Nyquist plots of the impedance for 4 different samples, from 20Hz to 2MHz. The imaginary part minimum is the resistance of the sample. The frequency goes from right to left. Most sample have a semi-circle on the left high frequency side. The samples with higher conductivity had the imaginary part minimum at the higher frequencies. The high conductivity samples showed less of the half circle. The interface semi-blocking impedance is set to $Z_i(\omega) = 33(iC_i\omega)^{-0.6}$ .

.

## 7.8 Conductivity — Temperature Dependence

### 7.8.1 Dry Samples

Temperature had a large effect on the conductivity. In Figure 36 we can see that the conductivity increased about three times when the temperature increased form 18 °C to 33°C. The 0.086 mol/kg LiTf sample however had almost no temperature dependence.

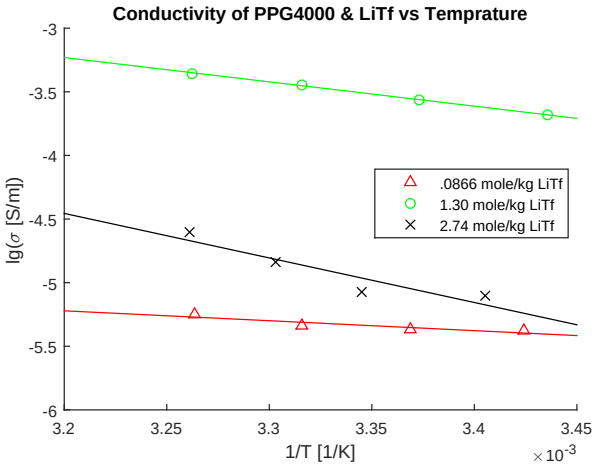



Figure 36: Conductivity vs temperature for different LiTf concentrations in PPG4000. The viscous 2.7 mol/kg LiTf sample has a high temperature dependence, and the low concentration 0.086 mol/kg sample has a low temperature dependence.

### 7.8.2 Samples With Water

The PPG4000-LiTf-Water samples also had a positive conductivity-temperature dependence as seen in Figure 37. The conductivity varied linearly. The curves are used to interpolate the conductivity at 23 °C for all samples. This interpolated value is used in the following chapters.

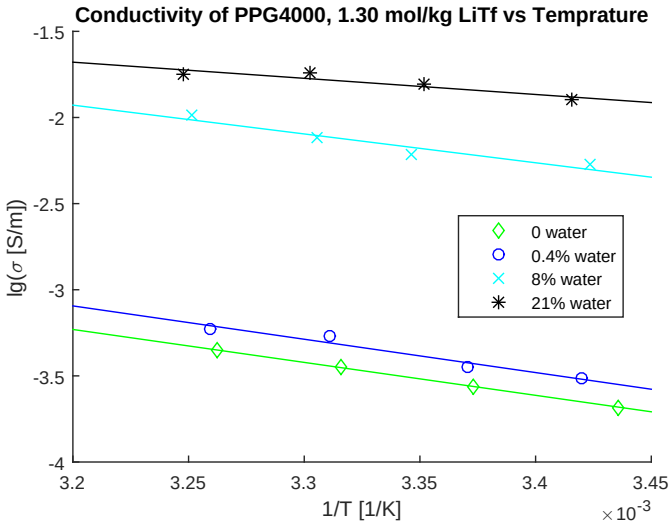



Figure 37: The conductivity of PPG4000, 0.63 mol/kg LiTf and water vs temperature. Higher water content has higher conductivity, but similar temperature dependence.

## 7.9 Conductivity — LiTf Concentration dependence

Figures 38 show the dependence of conductivity at 23 °C on LiTf concentration. The conductivity increases from a low $3.8 \cdot 10^{-8}$ S/m for pure PPG4000 to $2.9 \cdot 10^{-4}$ S/m at 0.63 mol/kg LiTf and then levels of and decreases to $8.4 \cdot 10^{-6}$ S/m at at 2.7 mol/kg LiTf. The viscosity increased with LiTf concentration, but was not measured quantitatively. Albinsson [9] used a model for ion pairs to explain the low molar conductivity at low concentrations. The viscosity measurements in the thesis[9] explain the low molar conductivity at high concentrations. The mobility of particles in fluids is inversely proportional to the viscosity, according to Stokes relationship. It is very reasonable to assume the increased viscosity is part of the explanation for the decreased conductivity beyond 1 mol/kg LiTf. The simple relationship (1), $\Lambda = \Lambda_0 - K\sqrt{c}$, doesn't work for this polymer electrolyte. Some kind of PPG4000-LiTf interaction decreases the activity in low concentrations, making the activity almost proportional to the concentration. For high concentrations, the relative conductivity decreases more in line with $\Lambda = \Lambda_0 - K\sqrt{c}$ .

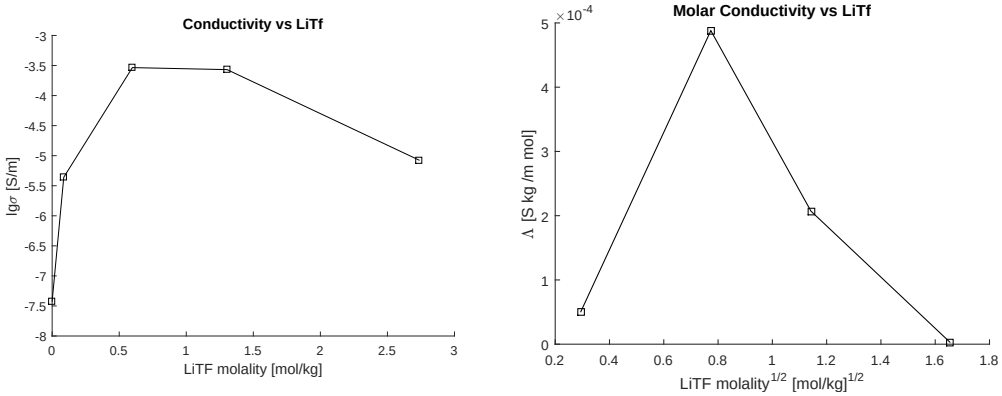



Figure 38: Conductivity vs LiTf concentration. The conductivity has a maximum at 1 mol/kg LiTf. The high concentration sample were viscous.

## 7.10 Conductivity — Water Content Dependence

Figure 39 shows that the water increased the conductivity at 23 °C for all LiTf concentrations. The increase was largest up to 7% water and then leveled off for all concentrations to approximately 14 mS/m. The 0.084 mol/kg LiTf sample conductivity increased from $4.4 \cdot 10^{-6}$ to $8.0 \cdot 10^{-5}$ S/m. The 2.7 mol/kg LiTf sample increased from $8.4 \cdot 10^{-6}$ to $1.5 \cdot 10^{-2}$ S/m. The medium concentration samples like 1.3 mol/kg increased from $2.9 \cdot 10^{-4}$ to $1.2 \cdot 10^{-2}$ S/m. The results from the $SO_3$ IR band show that that there are ion pairs in the dry samples. The $SO_3$ IR band also shows that the ion pairs are broken up by water. This explains the molar conductivity increase in the low and medium LiTf concentration samples. The high viscosity of the dry, high LiTf concentration samples explain their low conductivity. Adding water to the high LiTf concentration samples decreased the viscosity significantly, explaining the large increase in conductivity.

In the phase separated samples, the aqueous phase with its higher LiTf concentration will have orders of magnitude higher conductivity.[8]. This fact will make the conductivity of very sensitive to small variations in geometry. Measurements were made on one phase separated sample, but the resistance fluctuated between measurements. Figure 40 shows that the emulsion sample had a fluctuating conductivity, while the homogeneous sample had a stable temperature dependence. The thin thickness of the emulsified sample might exacerbate the fluctuations.

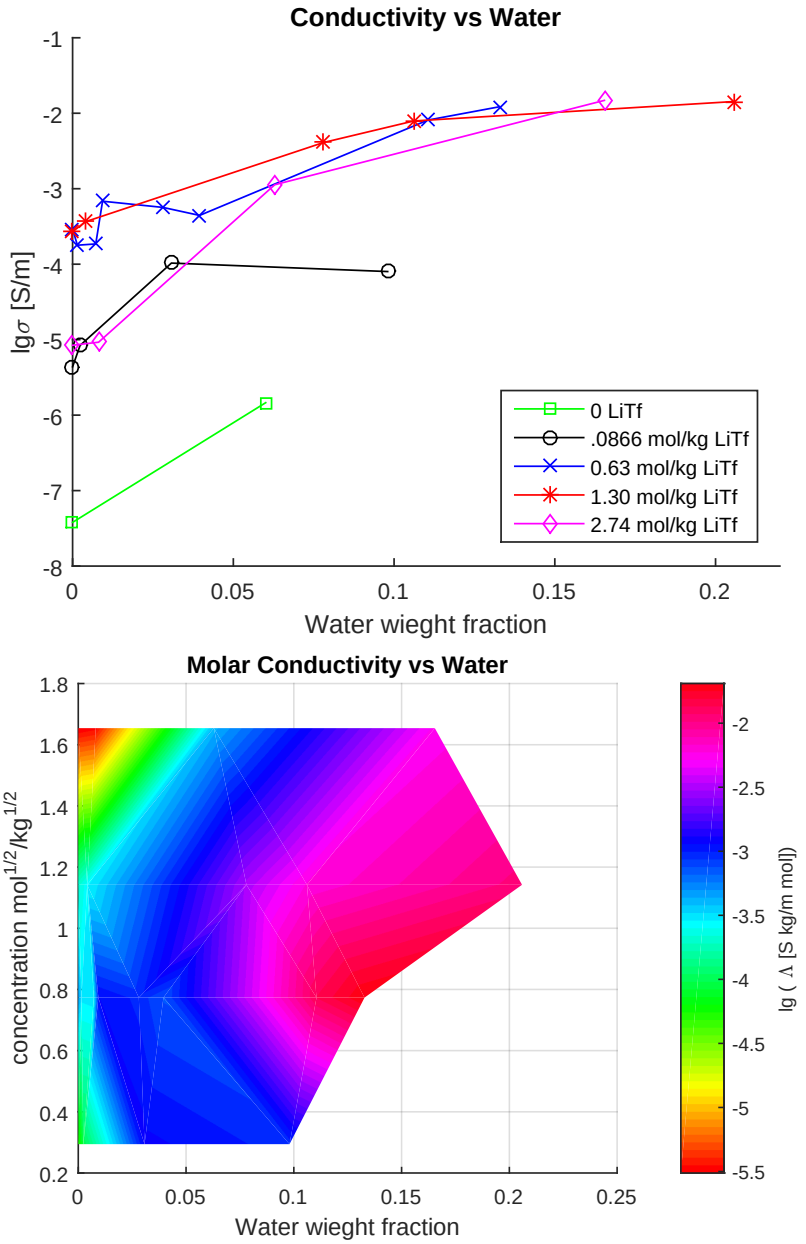



Figure 39: molar conductivity vs water for different LiTf concentrations in PPG4000. Interpolated to find the conductivity at 23 C and between sample concentrations. Note water increases the conductivity for all samples. The highest molar conductivity were 0.64 mol/kg LiTf, 13% water. The dry, high or low LiTf concentrations had the lowest conductivity.

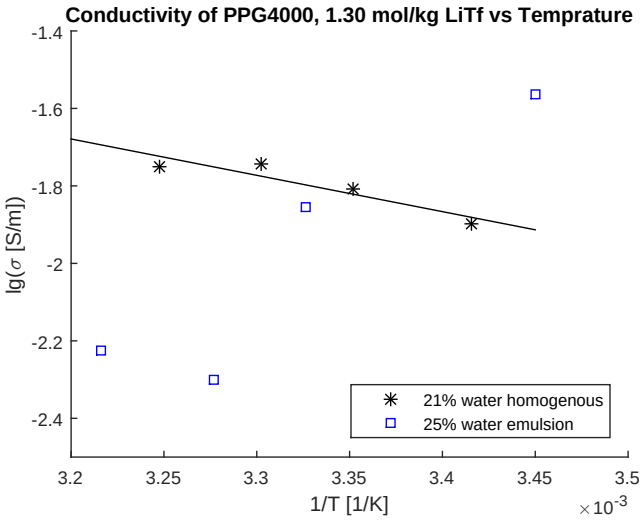



Figure 40: A comparison of temperature — conductivity dependence between an homogeneous and an emulsified sample. The emulsified sample was extremely thin (approx 0.03 mm).

## 7.11 Complex Permittivity — Frequency Dependence

Figure 41 shows the difference between the model and the results for the frequency dependent complex permittivity at 23°C. The model doesn't agree with the results for the high frequency, and gives a lower value for the plateau. This explains the lower value for $C_b$ in Figure 47. The value $C_b$ is fitted to the high frequency impedance, and gives an asymptotically constant permittivity. To model a dip in complex permittivity for frequencies higher than the plateau, the permittivity must be modeled with more than a capacitance. And a capacitance and a small resistance in series would be the simplest change. Figure 42 a suggestion for improvement of the model circuit.

Figure 43 shows permittivity values for different thicknesses of the same sample. We that there is an uncertainty in the sample thickness. Figure 44 show the frequency dependent complex permittivity of the samples. Some of the sample didn't have a conclusive plateau.

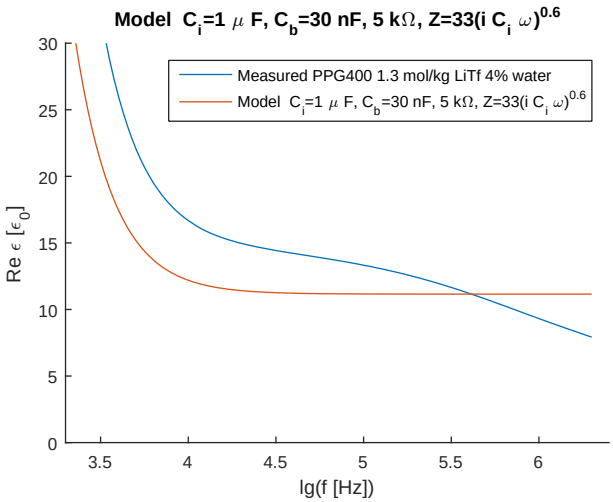



Figure 41: A frequency dependent complex permittivity comparison between model and results. The model doesn't agree for the high frequency, and gives a lower value for the plateau. The permittivity value of the model is the same as $dC_b/A$.

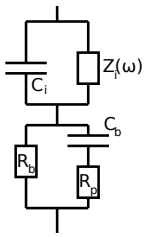



Figure 42: A suggestion to improve the circuit model. The resistance $R_p$ is very small.

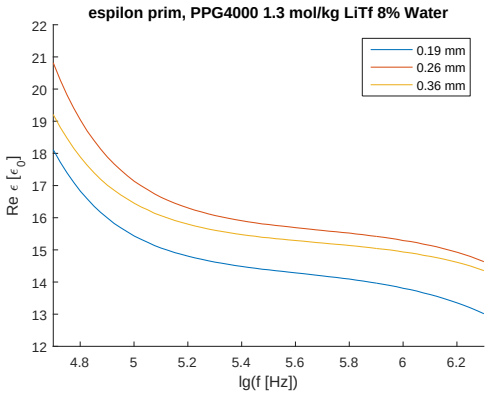



Figure 43: The real part of the frequency dependent complex permittivity, $\epsilon'$, for different thicknesses. Slight temperature variation. This shows the error from sample thickness

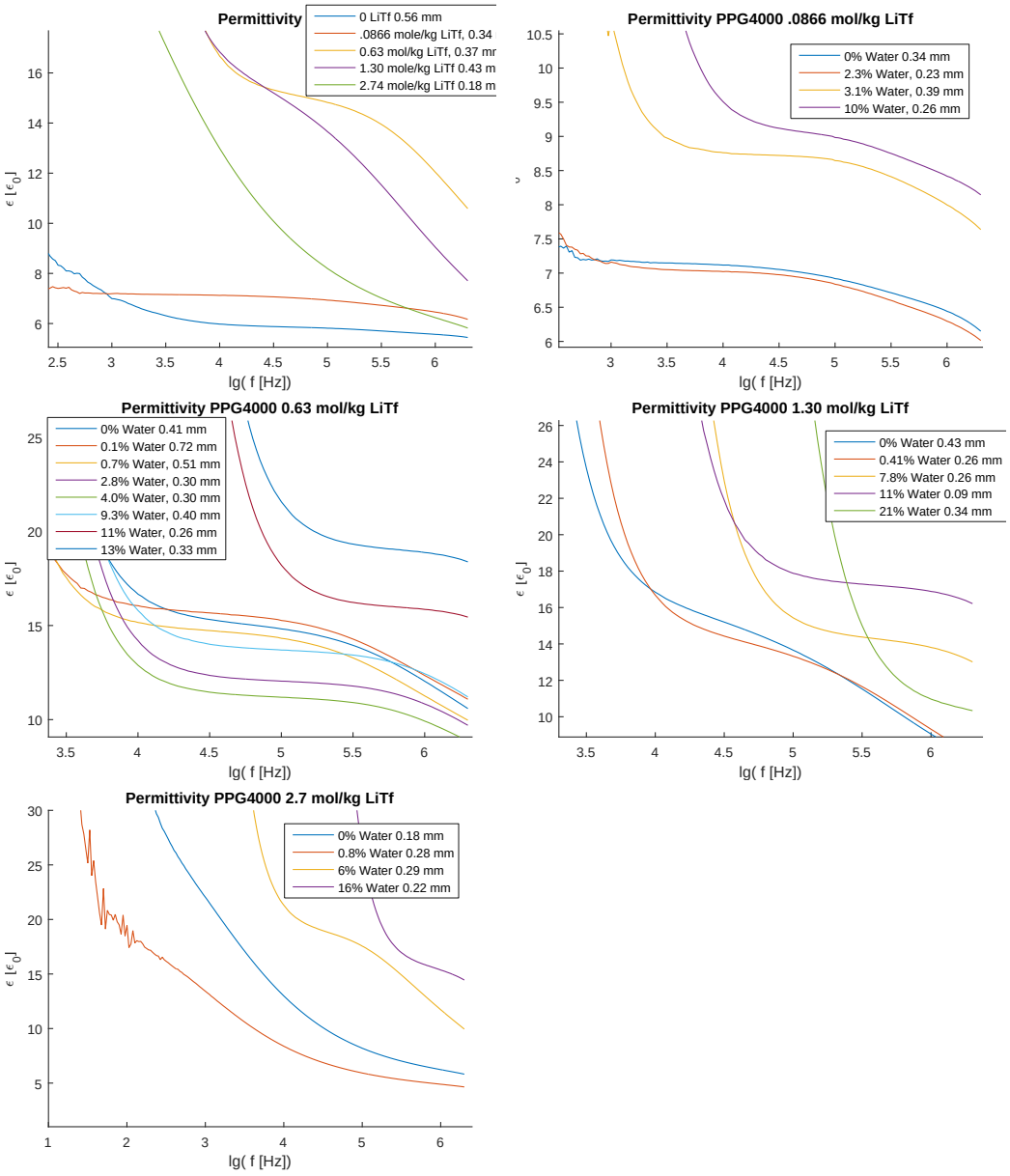



Figure 44: The real part of the frequency dependent complex permittivity, $\epsilon'$, of PPG4000 and LiTf. Some sample doesn't have a plateau.

## 7.12 Permittivity Value — LiTf and water concentration dependence

Figure 46 shows the permittivity values obtained from the complex permittivity. The permittivity value increased with LiTf concentration. Figure 47 shows the capacitor $C_b$ parametre from the model, compensated for size. The two methods for calculating the permittivity value agree for low LiTf concentrations, but disagree for high. For the 0.63 mol/kg LiTf, both show a minimum at 5% water. The disagreement between the permittivity methods can come from simplifications made in the model. Figure 45 shows how the the model permittivty value prediction diverges form the true permittivity value above 1 mol/kg LiTf.

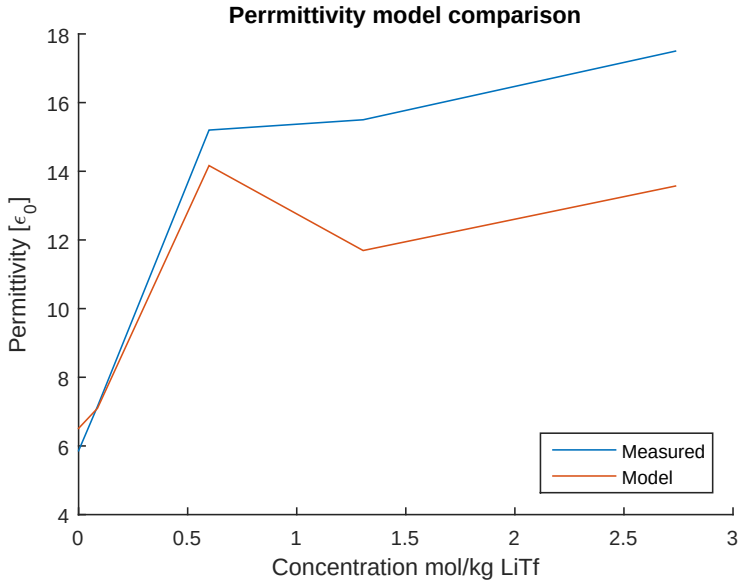



Figure 45: Permittivity value prediction from the model compared to the permittivty value from the complex permittivity.

The IR spectroscopy concludes that the dry electrolyte ions form into pairs and that water breaks up these ion pairs. Ion pairs are very interesting to the permittivity because they are strong dipoles. The conductivity decrease in low concentration is explained by ion pairs. The permittivy value doesn't tell the same story. The medium LiTf concentrations decrease respect to water could be explained by water breaking up ion pairs. The increase could be water it self increasing the permittivity values. The increase in permittivty value with LiTf concentration suggests the number of ion pairs increase. At the same time the low molar conductivity in low concentration

is large ratio of ion pairs. The formation of ion triplets or more complicated ion complexes would explain both the conductivity and permittivity value increase.

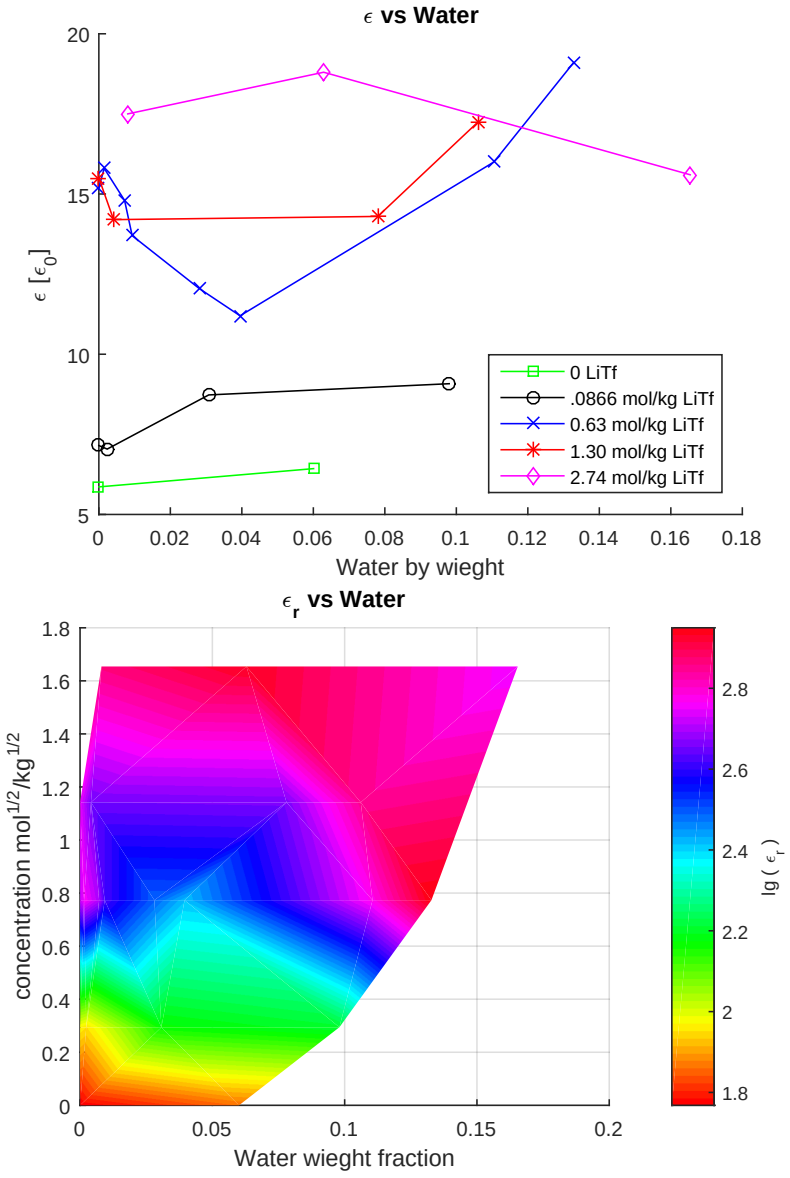



Figure 46: The permittivity value increased with LiTf concentration. Medium concentrations have minimums with respect to water.

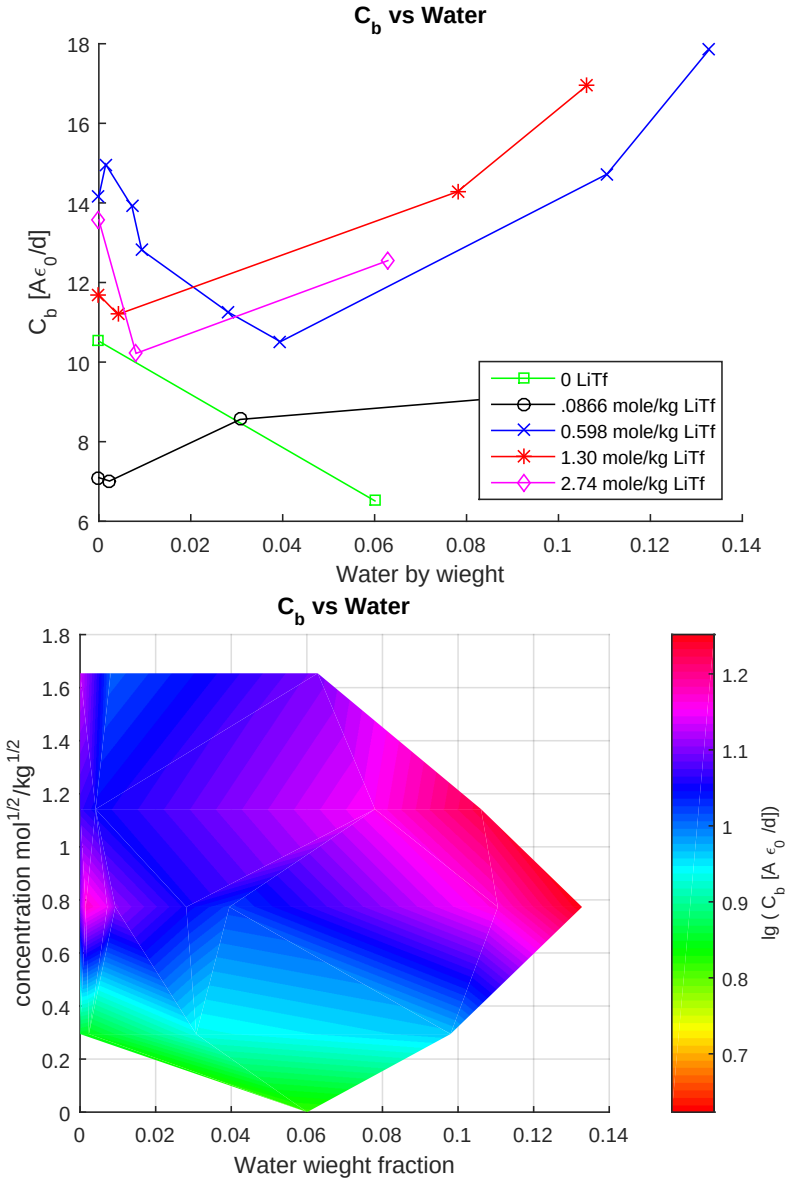



Figure 47: $d \cdot C_b * d/A/\varepsilon_0$ vs water for different LiTf concentrations in PPG4000.

# 8 Conclusion

Water increased the conductivity for all concentrations of LiTf in PPG4000. The conductivity increase in low concentration is explained be water breaking apart the ion pairs. The large increase in conductivity for high concentrations is explained by viscosity going from high to low. Several permittivity

measurements were inconclusive. However it was found that the 0.63 mol/kg LiTf sample had a permittivity minimum at 4% water by weight. Water breaking apart ion pairs is a process that could lower the permittivity. The circuit model predicted the impedance behaviour well, but it diverged with measurement for the highest frequency. This made the circuit model predict to low permittivty, with the error being worse for high LiTf concentrations. The impedance spectroscopy and circuit model was successful at calculating the conductivity. The method for drying and adding water was sufficient was hard to verify. PPG4000 dissolve 4 % water before separating into polymer phase and aqueous phase. Mixing in LiTf proportionally increases the amount of water that can be dissolved, up to 50% for 2.7 mol/kg LiTf. If more water is added the sample separates into PPG4000-LiTf-water and aqueous+LiTf phases. This behavior could be used to separate the PPG4000 and the LiTf. In open air PPG4000-LiTf absorb water to a seventh of the saturation content. The $SO_3$ stretch IR band show that $SO_3$ coordinates with OH from water or PPG4000. But in dry samples with limited OH form ion pairs. $SO_3$ stretch IR band shows that ion complexes are dominating at all LiTf concentration without water. The decrease ion pairs explain part of the conductivity increase with added water. The IR 1087/cm PPG4000 CO band of the 2.7 mol/kg LiTf sample showed that there is CO - $Li^+$ interaction. The increasing permittivity with LiTf concentration points to an increasing amount of ion pairs. The limited molecular interaction between PPG4000 and water in PPG4000-LiTf-water mixes, together with the phase separation into polymer phase and aqueous phase, leads to a simplified view that PPG4000-LiTf-water mixes can be seen as (PPG4000-LiTf)-(water-LiTf) mixes.

# A Appendix

## A.1 Method

Here follows a through motivation for the model introduced in 5. The interface is modeled as a capacitance, $C_i$, and the bulk and a resistance, $R_b$, and a capacitance, $C_b$, in parallel. We know that $C_i >> C_b$ and $|Z_i| > R_b$

$$Z(\omega) = \frac{1}{1/Z_i(\omega) + \mathrm{i}C_i\omega} + \frac{1}{1/R_b + \mathrm{i}C_b\omega}$$

$\nu_i = \frac{1}{C_i R_b}$ and $\nu_b = \frac{1}{C_b R_b}$

$$\frac{Z(\omega)}{R_b} = \frac{1}{R_b/Z_i(\omega) + \mathrm{i}\omega/\nu_i} + \frac{1}{1 + \mathrm{i}\omega/\nu_b}$$

We know that $C_i >> C_b$ and therefore $\nu_i << \nu_b$. If one assumes

$$\omega/\nu_i >> R_b/|Z(\omega)| \tag{5}$$

$$\frac{Z(\omega)}{R_b} = \frac{1}{\mathrm{i}\omega/\nu_i} + \frac{1}{1 + \mathrm{i}\omega/\nu_b}$$

$$\frac{Z(\omega)}{R_b} = -\mathrm{i}\nu_i/\omega + \frac{1}{1 + \omega^2/\nu_b^2} - \frac{\mathrm{i}\omega/\nu_b}{1 + \omega^2/\nu_b^2}$$

The imaginary part, the reactance, is

$$\frac{\mathfrak{Im}Z(\omega)}{R_b} = -\nu_i/\omega - \frac{\omega/\nu_b}{1 + \omega^2/\nu_b^2}$$

We further assume

$$\omega/\nu_b << 1 \tag{6}$$

The largest non vanishing terms are

$$\frac{\mathfrak{Im}Z(\omega)}{R_b} = -\frac{1}{\omega/\nu_i} - \omega/\nu_b$$

Which has a maximum at $\omega_R = \sqrt{\nu_i\nu_b} = \frac{1}{R\sqrt{C_i C_b}}$. This satisfies assumption (5) because

$$\frac{\sqrt{\nu_i\nu_b}}{\nu_i} >> 1 > R_b/|Z_i|$$

$\omega_R$ also satisfies assumption (6) because

$$\frac{\sqrt{\nu_i\nu_b}}{\nu_b} << 1$$

. The largest term in the real part of the impedance at this point is

$$\frac{Z(\omega)}{R_b} = 1$$

Giving us the ionic resistance. All measured samples contain this point.

lets look at $\omega_+$, a frequency higher then $\omega_R$. $R_b$, $Z$, $\omega_+$ and $\omega_R$ are known.

$$\frac{Z(\omega)}{R_b} = -\mathrm{i}\nu_i/\omega + \frac{1}{1+\omega^2/\nu_b^2} - \frac{\mathrm{i}\omega/\nu_b}{1+\omega^2/\nu_b^2} \tag{7}$$

Take the real part

$$\frac{\mathfrak{Re}Z(\omega_+)}{R_b} = \frac{1}{1+\omega_+^2/\nu_b^2}$$

Which solves $\nu_b$

$$1+\omega_+^2/\nu_b^2 = \frac{R_b}{\mathfrak{Re}Z(\omega_+)}$$

$$\omega_+/\nu_b = \sqrt{\frac{R_b}{\mathfrak{Re}Z(\omega_+)} - 1}$$

$$\nu_b = \frac{\omega_+}{\sqrt{\frac{R_b}{\mathfrak{Re}Z(\omega_+)} - 1}}$$

$$C_b = \frac{1}{R_b\omega_+}\sqrt{\frac{R_b}{\mathfrak{Re}Z(\omega_+)} - 1} \tag{8}$$

$$J = -i\omega\varepsilon E$$

$$J = \frac{AZ}{d}$$

$$\frac{\mathrm{i}d}{\omega * AZ} = \varepsilon$$

## A.2 Code

The code was written in matlab. Listed here are only the central functions used to find the result.

```
oxygen=15.99903;
carbon=12.0096;
hydrogen=1.00784;
lithium=6.938;
```

```
flourine=18.998403;
sulfur=32.059;
watermoleweight=2*hydrogen+oxygen;
litfmolewieght=lithium+carbon+3*oxygen+sulfur+3*flourine;
PGGmonomermolewieght=3*carbon+oxygen+6*hydrogen;
weightprocL=[1.3 4 9 17 30]/100;
MoleratioL=PGGmonomermolewieght/litfmolewieght*weightprocL./(1-weightprocL);
MolarityL=1/litfmolewieght*weightprocL./(1-weightprocL)*1000; %g to kg
weightprocW=[1.3 3 9 17 25]/100;
MoleratioW=PGGmonomermolewieght/watermoleweight*weightprocW./(1-
weightprocW);
MolarityW=1/watermoleweight*weightprocW./(1-weightprocW)*1000;
function [Cond,diel]=conductivity2(A,d,minres,plotpromt)
    Realpart=A(:,1);  %Impedance
    Imagpart=A(:,2);
    W111=importdata('E498x034.Template Agilent E4980Acommatopoint.csv');
    Freq=W111(:,2);  %Frequency
    w=2*pi*Freq;  %angular frequancy
    d0=24.14;%  Sample thickness mm
    Diametre=10.293; %mm
    Radius=Diametre/2;
    Area=pi*Radius^2; %mm^2
    [~,j]=min(-Imagpart+max(-Imagpart)*(Realpart<minres)); % Find (-
)Impedance minimum
    A2res=Realpart(j);  % This point has the bulk resistance
    Cond=(d-d0)/Area/A2res*1000;  %Calculate conductivity
    [~,k]=min(Imagpart(j:end)); % Find (-)Impedance maximum for permitivity
    m=k+j-1; %Impedance maximum frequency
    diel=(d-d0)/Area*1000*sqrt(A2res/Realpart(m)-1)/w(m)/A2res/8.854187817e-
12;  %relative permi
    if plotpromt==1 %Plot Options
        hold on
        plot(Realpart,-Imagpart) % Negative imaginary part
        plot(A2res,0,'x')
        xlabel('Re Z [\Omega]')
        ylabel('-Im Z [\Omega]')
    elseif plotpromt==2  %Plot Comparison to full model
        hold on
        plot(Realpart,-Imagpart)
        %plot(A2res,0,'x')
        %Zi=(20)*A2res;
```

```
        Cb=sqrt(A2res/Realpart(m)-1)/w(m)/A2res;  %Find bulk capacitance to plug
        Ci=1/(A2res^2*w(j)^2*Cb);   %Find interface capacitance to plug into mod
        Z=(1+0*Freq)./(0.03*(1i*Ci*w).^0.6+1i*Ci*w)+(1+0*w)./(1/A2res+1i*Cb*w);
        Zre=real(Z);
        Zim=imag(Z);
        plot(Zre,-Zim) % Negative imaginary part
        xlabel('Re Z [\Omega]')
        ylabel('Im Z [\Omega]')
    elseif plotpromt==3
        hold on
        if d<24.35
            plot(log10(Freq),atan2(Imagpart,Realpart))
        else
            plot(log10(Freq),atan2(Imagpart,Realpart),'--')
        end
        xlabel('lg \omega [Hz]')
        ylabel('\phi [1]')
        axis([log10(Freq(1)) 8 -pi/2 0])
    elseif plotpromt==4
        hold on
        %plot(Realpart,-Imagpart)
        %plot(A2res,0,'x')
        Cb=sqrt(A2res/Realpart(m)-1)/w(m)/A2res;
        Ci=1/(A2res^2*w(j)^2*Cb);
        Zi=(1+0*Freq)./((1+0*w)./(Realpart+1i*Imagpart-(1+0*w)./(1/A2res+1i*Cb*F
1i*Ci*w);
        Zire=real(Zi);
        Ziim=imag(Zi);
        plot(Zire,Ziim)
        Zmod=1/(0.0003*(1i*Ci*w).^0.5);
        Zmre=real(Zmod);
        Zmim=imag(Zmod);
        plot(Zmre,Zmim)
        xlabel('Re Z [\Omega]')
        ylabel('Im Z [\Omega]')
        legend('Measured','Model Z_i=33 (i C_i \omega)^{-0.6}','location','northw
    elseif plotpromt==5

        hold on
        q=(d-d0)/(Area/1000)./(w)/8.854187817e-12;
        epsprim=-Imagpart./(Realpart.^2+Imagpart.^2).*q;
```

```
        plot(log10(Freq),epsprim)
    end

end
```

```
function weigthratios=mixing(weight1,weight2,weigthratios1,weigthratios2)
    weigthratios=(weight1*weigthratios1+weight2*weigthratios2)/(weight1+weight2)
end
```

# References


[1] Sigma-Aldrich, Poly(propylene glycol) product page. https://www.sigmaaldrich.com/catalog/product/aldrich/202355?lang=en&region=SE https://www.sigmaaldrich.com/catalog/product/aldrich/81350?lang=en&region=SE

[2] Stuart B, *Infrared spectroscopy fundamentals and applications.* John Wiley & Sons; 2004

[3] Sigma-Aldrich, Lithium Triflate product page. https://www.sigmaaldrich.com/catalog/product/aldrich/481548?lang=en&region=SE

[4] Ferry A., Minmin T. *Influence of Hydroxyl Groups on the Ionic Speciation and Ionic Conductivity in Complexs of Poly(Propylene gycol)(4000) and LiCF3SO3 salt.* Macromolecules, Vol. 30, No. 4; 1997.

[5] Bishop A. G., MacFarlane D. R. et.al. *Triflate ion association in plasticrzed polymer eletrolytes.* Solid State Ionics (85) p.129-135; 1996

[6] David R. Lide, ed., *CRC Handbook of Chemistry and Physics*, 89th ed., CRC Press/Taylor and Francis, Boca Raton, FL; 2009.

[7] Murrell J. N., Jenkins A. D., *Properties of Liquids and Solutions* John Wiley & Sons 1982 2nd ed. Ch 9

[8] Hamrin A.; Scott E., *Aqueous Electrolytes for Next Generation Batteries* [Master Thesis]. Chalmers University of Technology; 2018.

[9] Albinsson I. *Dielectric and conductivity studies of polymer electrolytes.* [PhD Thesis] Göteborg: Chalmers University of Technology and Gothenburg University; 1994.

[10] Sengwa R. J. *Dielectric behaviour and relaxation in poly(propylene glycol)-water mixtures studied by time domain reflectometry.* Polymer International. 2004; (53), p.744-748.

[11] Ferry A. and Jacobsson P. Stevens J. R., *Studies of Ionic Interactions in Poly(propylene glycol)4000 Complexed with Triflate Salts.* Journal of Physical Chemistry; 1996, (100): p.12574-12582

[12] Atkins P., *Physical Chemistry* Oxford University Press 6th ed., Ch 29; 1998

[13] Bergström P. Å., Lindgren J. *An infrared study of the hydration of the triflate ion (CF3SO3) in aqueous solution* Journal of Molecular Structure; 1990, (239): p.103-111

[14] Simon A., DE102004025448B4 [Patent]; 2007 `https://patents.google.com/patent/DE102004025448B4/de`